A Sarrus-like overconstrained eight-bar linkage and its associated Fulleroid-like platonic deployable mechanisms

Xiu, Haohua, Wang, Kunyang, Wei, Guowu, Ren, Lei and Dai, Jian S

Title	A Sarrus-like overconstrained eight-bar linkage and its associated Fulleroid-like platonic deployable mechanisms
Authors	Xiu, Haohua, Wang, Kunyang, Wei, Guowu, Ren, Lei and Dai, Jian S
Type	Article
URL	This version is available at: http://usir.salford.ac.uk/49751/
Published Date	2018

A Sarrus-like Overconstrained Eight-bar Linkage and Its Associated Fulleroid-like Platonic Deployable Mechanisms *

Haohua Xiu[1], Kunyang Wang[2], Guowu Wei[3], Lei Ren[2], Jian S. Dai[4]

Abstract

This paper for the first time presents an overconstrained spatial eight-bar linkage and its application to the synthesis of a group of Fulleroid-like deployable Platonic mechanisms. Structure of the proposed eight-bar linkage is introduced, and constrain and mobility of the linkage are revealed based on screw theory. Then by integrating the proposed eight-bar linkage into Platonic polyhedron bases, synthesis of a group of Fulleroid-like deployable Platonic mechanism is carried out and illustrated by the synthesis and construction of a Fulleroid-like deployable tetrahedral mechanism. Further, mobility of the Fulleroid-like deployable Platonic mechanisms is formulated via constraint matrices by following Kirchhoff's circulation law for mechanical networks, and kinematics of the mechanisms is presented with numerical simulations illustrating the intrinsic kinematic properties of the group of Fulleroid-like deployable Platonic mechanisms. In addition, a prototype of the Fulleroid-like deployable spherical-shape hexahedral mechanism is fabricated and tested verifying mobility and kinematic characteristics of the proposed deployable polyhedral mechanisms. Application of the proposed deployable Platonic mechanisms is demonstrated in the development of a transformable quadrotor. This paper hence presents a novel overconstrained spatial eight-bar linkage and a new geometrically intuitive method for synthesizing Fulleroid-like regular deployable polyhedral mechanisms that have great potential applications in deployable, reconfigurable, and multi-functional robots.

Introduction

Overconstrained mechanisms, from the simple four-bar Bennet linkage (1) to the very complex deployable truncated icosahedral mechanism (2), have never lost their fascination to researchers in the science and engineering research communities. In most of the cases, the topology of an overconstrained mechanism might indicate rigidity but it is movable, or it has more mobility than the one its topology predicts. Hence, such mechanisms have greater mobility than the number that is calculated through the Grübler-Kutzbach formula (3).

As pointed out by Wittenburg (4), the early history for the search of overconstrained mechanisms was marked by chance discoveries and by ingenuity; such as the Sarrus linkage (5). In the family of overconstrained linkages, there is one type of linkages that are constructed by purely using revolute (R) joints. These include the four-bar Bennett linkage (1), the five-bar Goldberg linkage (6), the five-bar and six-bar Myard linkages (7; 8), a number of six-bar overconstrained linkages (9; 10; 11; 12; 13; 14; 15; 16; 17; 18) particularly the Bricard linkages (9) and Schatz linkage (11), and the seven-bar Dietmaier mechanism (19). Nevertheless, to the best of the authors' knowledge, no overconstrained spatial eight-bar linkage has been reported so far.

By integrating and merging the above are single-loop spatial overconstrained linkages, different kinds of multi-loop overconstrained mechanisms can be constructed.

Based on Bennett linkages, assemblies of deployable structures were constructed in forms of arches and cylindrical profile (20), integrating Myard linkage, large scale spatial deployable networks were constructed (21), and by combining and assembling Bricard and Myard linkages, multi-loop deployable mechanisms were developed (22). Further, by implanting the four-bar Bennett loops into regular polyhedral bases, a group of regular spherical polyhedral linkages which belong to the deployable polyhedral mechanisms (DPMs) were synthesized (23).

The deployable polyhedral mechanisms (DPMs) are mechanisms that are synthesized and constructed by implanting elementary kinematic chains into the faces, edges and vertices of polyhedra. Most of them are symmetric and

[1] School of Mechanical Science and Engineering, Jilin University, Changchun 130000, China
[2] School of Mechanical, Aerospace and Civil Engineering, The University of Manchester, Manchester M13 9PL, UK
[3] School of Computing, Science and Engineering, University of Salford, Salford M5 4WT, UK
[4] Centre for Robotics Research, King's College London, London WC2R 2LS, UK

Corresponding author:
Guowu Wei, School of Computing, Science and Engineering, University of Salford, Salford, M5 4WT, UK
Lei Ren, School of Mechanical, Aerospace and Civil Engineering, The University of Manchester, Manchester M13 9PL, UK
Email: g.wei@salford.ac.uk, and lei.ren@manchester.ac.uk

regular overconstrained mechanisms. As pioneering work, Bricard proposed flexible p olyhedrons (9) a nd Verheyen (24; 25) presented the expandable polyhedral structures which were coined "Jitterbug transformers". Then, Wohlhart (26; 27; 28; 29; 30; 31; 32; 33) proposed different synthesis methods leading to the generation of the "Turning Tower", the "Breathing Ball", and the "Star-cube", etc. Agrawal et al. (34) proposed a simple approach for constructing expanding polyhedrons based on prismatic joints which could preserve their shape because of the rigidity of the vertices. Chen et al.(35; 36; 37) investigated the two-Orbit switch-pitch structures and applied the group-theory-based approach to the mobility analysis of symmetric overconstrained structures. Gosselin and Gagnon-Lachance (38) developed a family of expandable polyhedral mechanisms based on Platonic solids, pentagonal prism solids and gyrobifastigium solids by integrating 1-DOF regular polygon-shaped planar linkages into the faces of the polyhedral solids and assembling them with spherical joints at the vertices of the polyhedral solids. Laliberté and Gosselin (39) then proposed the concept of PAFs (polyhedrons with articulated faces) and constructed a series of polyhedral linkages/structures from Platonic solids, Archimedean solids, Johnson solids and Rhombic solids. Kiper et al. (40) presented analytical synthesis methods of constructing Fulleroid-like linkages based on the Fulleroid (28; 41) and polyhedral linkages (42) possessing Cardan motion which belong to the special cases of the Röschel's unilaterally closed mechanisms (43; 44; 45). Li et al. (46) constructed deployable polyhedral mechanisms based on extended parallelogram mechanisms, which then led to the development of reconfigurable deployable polyhedral mechanism (47; 48; 49) . Further, Wei and Dai (50; 51; 52; 53; 54; 2; 55) found that by integrating two fundamental kinematic linkages, i.e. one PRRP (P denotes prismatic joint and R stands for revolute joint) chain and one spatial eight-bar linkage, into faces, edges and vertices of the polyhedrons, deployable polyhedral mechanisms with radially reciprocating motions can be synthesized and constructed.

In the study of DPMs, the Fulleroid-like polyhedral mechanisms have stimulated particular interest. Wohlhart (56; 28) synthesized and investigated kinematics and dynamics of the mechanisms; Kiper (57) synthesized the Fulleroid-like dipyramidal and stellated polyhedral linkages; and Röschel (58) studied self-motions of the Fulleroid-like mechanisms. In this paper, a Sarrus-like overconstrained eight-bar linkage is presented and a geometrically intuitive method is proposed for the synthesis of a group of Fulleroid-like Platonic deployable mechanisms. Structure, mobility and kinematics of the proposed eight-bar linkage are investigated and synthesis of Fulleroid-like deployable Platonic mechanisms is presented; illustrating by synthesizing and constructing a Fulleroid-like deployable tetrahedral mechanism. Further, mobility and kinematics of the proposed Fulleroid-like deployable Platonic mechanisms are addressed. In addition, application of the proposed deployable mechanisms is addressed through the innovative development of a deployable quadcopter based on the deployable hexahedral mechanism.
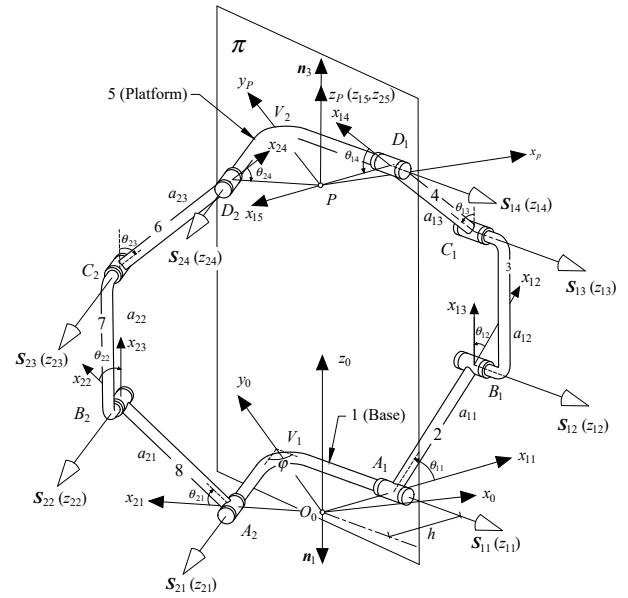
Figure 1. A Sarrus-like overconstrained spatial eight-bar linkage and its geometry

Characterisation of a Sarrus-like Overconstrained Eight-Bar Linkage

A Sarrus-like overconstrained eight-bar linkage is introduced in this section and its structure equation is established. Then, mobility of this linkage is calculated using the screw-loop equations (51).

A Sarrus-like Overconstrained Spatial Eight-Bar Linkage

Following the study of the dual-plane-symmetric spatial eight-bar linkage in (50), a novel Sarrus-like overconstrained spatial eight-bar linkage is proposed in this paper. Fig. 1 illustrates the structure of the new spatial eight-bar linkage. Treating it as a two-limb parallel mechanism, it consists of two congruent isosceles V-shaped links one (link 5) as platform and the other one (link 1) as base. Each limb contains four parallel revolute joints which are connected by three binary links, the two revolute joints in one end of each limb are connected by the aforementioned V-shaped base and the other two joints in the other end of each limb are connected by the V-shaped platform. Both angles between the axes of joints A_1 and A_2 in the base, and between the axes of joints D_1 and D_2 in the platform are φ. Lengths of the links satisfy $a_{11} = a_{21}$, $a_{12} = a_{22}$, $a_{13} = a_{23}$. The linkage is symmetric with respect to a plane π that is formed by normals n_1 and n_3 of the base and the platform. The normal n_1 of the R-R dyad V_1 passes through bisector of angle φ between joints A_1 and A_2, and the normal n_3 of the R-R dyad V_3 lies on the bisector of the angle between joints D_1 and D_2.

This eight-bar linkage is similar to the Sarrus linkage (5), and by comparison with the Sarrus linkage, each limb of the linkage has one extra revolute joint together with an extra link; and similar to the Sarrus linkage, this spatial eight-bar linkage is also an overconstrained one whose mobility is to be formulated and identified in the following section.

Structure Equation of the Eight-bar Linkage

Referring to Fig. 1, in order to formulate structure equations and characterise the kinematics of the proposed linkage, a global coordinate frame $\{O_0, x_0, y_0, z_0\}$ is attached to the V-shaped base at point O_0, locating at the intersection of the y_0-axis and the x_{11}-axis on the plane of the V-shaped base; with the y_0-axis aligned with the bisector of angle φ and the x_{11}-axis perpendicular to joint A_1.

Similarly, a coordinate frame $\{O_p, x_p, y_p, z_p\}$ is attached to the V-shaped platform with the y_p-axis aligned with the bisector of angle φ and the z_p-axis perpendicular to the plane of the V-shaped platform. The eight-bar linkage is decomposed into two limbs as limb 1 (A_1, B_1, C_1, D_1, P) and limb 2 (A_2, B_2, C_2, D_2, P) as aforementioned. Local coordinate frames of each joint are attached to the kinematic joints in such a manner that the z_{jk}-axis directs along the axis of the jkth joints. Link lengths and twist angles are defined as a_{jk} and α_{jk}, respectively with the relations that $a_{11} = a_{12} = a_{13} = a_{21} = a_{22} = a_{23} = a$, joints angles and link offsets are denoted as θ_{jk} and d_{jk}; In these terms, the first subscript j is used to distinguish the two limbs and the second subscript k is used to number the joints in the two limbs. Further, assigning the distance between joint A_1 and O_0 as h, by following the distal variant Denavit-Hartenberg convention (59), the link and joint parameters can be obtained readily.

In the two open limbs, transformation matrices $\mathbf{G_1}$ and $\mathbf{G_2}$ represent the transformations of frames $\{A_1, x_{11}, y_{11}, z_{11}\}$ and $\{A_2, x_{21}, y_{21}, z_{21}\}$ in limb 1 and limb 2 with respect to the reference coordinate frame and given as $\mathbf{G_1} = [z_0(\varphi/2, 0)][x_0(\pi/2, h)]$, $\mathbf{G_2} = [z_0(\pi - \varphi/2, 0)][x_0(-\pi/2, h)]$, respectively. And using the D-H parameters, homogeneous transformation matrix between two adjacent local frames is given as

$$\mathbf{T}_{jk} = [z_{jk}(\theta_{jk}, d_{jk})][x_{j,k+1}(\alpha_{jk}, a_{jk})] \tag{1}$$

where $j = 1, 2$, $k = 1, 2, 3, 4$. Further, given the transformation matrices $\mathbf{H_1}$ and $\mathbf{H_2}$ defined as $\mathbf{H_1} = [z_{15}(\pi - \varphi/2, 0)][x_{15}(0, 0)]$ and $\mathbf{H_2} = [z_{25}(\varphi/2, 0)][x_{25}(0, 0)]$, which provides the transformation of the frame P, x_p, y_y, z_p locating at the common point P to the last local coordinate frames $\{x_{15}, y_{15}, z_{15}\}$ and $\{x_{25}, y_{25}, z_{25}\}$. Integrating the transformation matrices, the structure equation for each open limb can be given as follows:

For limb 1 it has

$$\mathbf{D_1} = \mathbf{G_1}\mathbf{T}_{11}\mathbf{T}_{12}\mathbf{T}_{13}\mathbf{T}_{14}\mathbf{H_1} \tag{2}$$

and for limb 2 it has

$$\mathbf{D_2} = \mathbf{G_2}\mathbf{T}_{21}\mathbf{T}_{22}\mathbf{T}_{23}\mathbf{T}_{24}\mathbf{H_2} \tag{3}$$

Hence, the structure equation of the closed-loop eight-bar linkage can be expressed as

$$\mathbf{G_1}\mathbf{T}_{11}\mathbf{T}_{12}\mathbf{T}_{13}\mathbf{T}_{14}\mathbf{H_1} = \mathbf{G_2}\mathbf{T}_{21}\mathbf{T}_{22}\mathbf{T}_{23}\mathbf{T}_{24}\mathbf{H_2} \tag{4}$$

For Eq. (4), the homogeneous coordinates for joints A_j to D_j $(j = 1, 2)$ in two limbs are derived as follows.

Homogeneous coordinates of joint A_j at point A_j are

$$\mathbf{A}_j = \mathbf{G}_j = \left[\begin{array}{cccc} \boldsymbol{x}_{Aj} & \boldsymbol{y}_{Aj} & \boldsymbol{z}_{Aj} & \boldsymbol{p}_{Aj} \\ 0 & 0 & 0 & 1 \end{array} \right] \tag{5}$$

homogeneous coordinates of joint B_j at point B_j are

$$\mathbf{B}_j = \mathbf{G}_j\mathbf{T}_{j1} = \left[\begin{array}{cccc} \boldsymbol{x}_{Bj} & \boldsymbol{y}_{Bj} & \boldsymbol{z}_{Bj} & \boldsymbol{p}_{Bj} \\ 0 & 0 & 0 & 1 \end{array} \right] \tag{6}$$

homogeneous coordinates of joint C_j at point C_j are

$$\mathbf{C}_j = \mathbf{G}_j\mathbf{T}_{j1}\mathbf{T}_{j2} = \left[\begin{array}{cccc} \boldsymbol{x}_{Cj} & \boldsymbol{y}_{Cj} & \boldsymbol{z}_{Cj} & \boldsymbol{p}_{Cj} \\ 0 & 0 & 0 & 1 \end{array} \right] \tag{7}$$

homogeneous coordinates of joint D_j at point D_j are

$$\mathbf{D}_j = \mathbf{G}_j\mathbf{T}_{j1}\mathbf{T}_{j2}\mathbf{T}_{j3} = \left[\begin{array}{cccc} \boldsymbol{x}_{Dj} & \boldsymbol{y}_{Dj} & \boldsymbol{z}_{Dj} & \boldsymbol{p}_{Dj} \\ 0 & 0 & 0 & 1 \end{array} \right] \tag{8}$$

Mobility of the Eight-bar Linkage

Based on the coordinates of positions and directions of the joint axes for the joints obtained in Section , joint screws of the eight-bar linkage can be formulated. Directions of the joint screws can be directly inherited from Eqs. (5)-(8) as $\boldsymbol{s}_{Ai} = \boldsymbol{z}_{Ai}$, $\boldsymbol{s}_{Bi} = \boldsymbol{z}_{Bi}$, $\boldsymbol{s}_{Ci} = \boldsymbol{z}_{Ci}$, and $\boldsymbol{s}_{Di} = \boldsymbol{z}_{Di}$, and the arbitrary points on the screw axes can be given as $\boldsymbol{r}_{Ai} = \boldsymbol{p}_{Ai}$, $\boldsymbol{r}_{Bi} = \boldsymbol{p}_{Bi}$, $\boldsymbol{r}_{Ci} = \boldsymbol{p}_{Ci}$, and $\boldsymbol{r}_{Di} = \boldsymbol{p}_{Di}$. Thus according to the screw for a revolute joint defined as $\boldsymbol{S} = (\boldsymbol{s}; \boldsymbol{r} \times \boldsymbol{s})$, motion-screw system of limb 1 can be given as

$$\mathbb{S}_1 = \begin{cases} \boldsymbol{S}_{A1} = \left[\begin{array}{cccccc} \sin(\varphi/2) & -\cos(\varphi/2) & 0 & 0 & 0 & -h \end{array} \right]^{\mathrm{T}} \\ \boldsymbol{S}_{B1} = \left[\begin{array}{cccccc} \sin(\varphi/2) & -\cos(\varphi/2) & 0 & p_{B1} & q_{B1} & r_{B1} \end{array} \right]^{\mathrm{T}} \\ \boldsymbol{S}_{C1} = \left[\begin{array}{cccccc} \sin(\varphi/2) & -\cos(\varphi/2) & 0 & p_{C1} & q_{C1} & r_{C1} \end{array} \right]^{\mathrm{T}} \\ \boldsymbol{S}_{D1} = \left[\begin{array}{cccccc} \sin(\varphi/2) & -\cos(\varphi/2) & 0 & p_{D1} & q_{D1} & r_{D1} \end{array} \right]^{\mathrm{T}} \end{cases} \tag{9}$$

and motion-screw system of limb 2 can be written as

$$\mathbb{S}_2 = \begin{cases} \boldsymbol{S}_{A2} = \left[\begin{array}{cccccc} -\sin(\varphi/2) & -\cos(\varphi/2) & 0 & 0 & 0 & h \end{array} \right]^{\mathrm{T}} \\ \boldsymbol{S}_{B2} = \left[\begin{array}{cccccc} -\sin(\varphi/2) & -\cos(\varphi/2) & 0 & p_{B2} & q_{B2} & r_{B2} \end{array} \right]^{\mathrm{T}} \\ \boldsymbol{S}_{C2} = \left[\begin{array}{cccccc} -\sin(\varphi/2) & -\cos(\varphi/2) & 0 & p_{C2} & q_{C2} & r_{C2} \end{array} \right]^{\mathrm{T}} \\ \boldsymbol{S}_{D2} = \left[\begin{array}{cccccc} -\sin(\varphi/2) & -\cos(\varphi/2) & 0 & p_{D2} & q_{D2} & r_{D2} \end{array} \right]^{\mathrm{T}} \end{cases} \tag{10}$$

where, the moment elements p, q and r in the above motion-screw systems are listed in Appendix A.

Calculating the reciprocal of $\mathbb{S}_1$ gives constraint-screw system of limb 1 as

$$\mathbb{S}_1^r = \begin{cases} \boldsymbol{S}_{11}^r = \left[\begin{array}{cccccc} 0 & 0 & 0 & \cos(\varphi/2) & \sin(\varphi/2) & 1 & 0 \end{array} \right]^{\mathrm{T}} \\ \boldsymbol{S}_{12}^r = \left[\begin{array}{cccccc} 0 & 0 & 0 & 0 & 0 & 1 \end{array} \right]^{\mathrm{T}} \end{cases} \tag{11}$$

Similarly, calculating the reciprocal screw of $\mathbb{S}_2$ gives constraint-screw system of limb 2 as

$$\mathbb{S}_2^r = \begin{cases} \boldsymbol{S}_{21}^r = \left[\begin{array}{cccccc} 0 & 0 & 0 & -\cos(\varphi/2) & \sin(\varphi/2) & 1 & 0 \end{array} \right]^{\mathrm{T}} \\ \boldsymbol{S}_{22}^r = \left[\begin{array}{cccccc} 0 & 0 & 0 & 0 & 0 & 1 \end{array} \right]^{\mathrm{T}} \end{cases} \tag{12}$$

Referring to (60), the platform constraint-screw multiset is the combination of the two constraint-screw systems of the two limbs, which is

$$\langle \mathbb{S}^r \rangle = \mathbb{S}_1^r \uplus \mathbb{S}_2^r \tag{13}$$

where card $\langle \mathbb{S}^r \rangle = 4$. However, $\langle \mathbb{S}^r \rangle$ only contains three linearly independent screws, a non-unique basis for the subspace of $\mathbb{S}^r$ can be selected as

$$\mathbb{S}^r = \begin{cases} \boldsymbol{S}_1^r = \begin{bmatrix} 0 & 0 & 0 & 1 & 1 & 0 \end{bmatrix}^T \\ \boldsymbol{S}_1^r = \begin{bmatrix} 0 & 0 & 0 & -1 & 1 & 0 \end{bmatrix}^T \\ \boldsymbol{S}_2^r = \begin{bmatrix} 0 & 0 & 0 & 0 & 0 & 1 \end{bmatrix}^T \end{cases} \tag{14}$$

where $\mathbb{S}^r$ gives a basis for a constraint-screw system of the platform.

Taking reciprocal of $\mathbb{S}^r$ gives the platform motion-screw system $\mathbb{S}_f$ with a basis

$$\mathbb{S}_f = \begin{cases} \boldsymbol{S}_{f1} = \begin{bmatrix} 0 & 0 & 0 & 1 & 0 & 0 \end{bmatrix}^T \\ \boldsymbol{S}_{f2} = \begin{bmatrix} 0 & 0 & 0 & 0 & 1 & 0 \end{bmatrix}^T \\ \boldsymbol{S}_{f3} = \begin{bmatrix} 0 & 0 & 0 & 0 & 0 & 1 \end{bmatrix}^T \end{cases} \tag{15}$$

which is the span of each of the limb motion-screw system $\mathbb{S}_j, j = 1, 2$.

Equation (15) indicates that the platform of the eight-bar linkage has three degrees of freedom which are respectively translations along the x_0-axis, y_0-axis and z_0-axis of reference coordinate system. This indicates that the proposed eight-bar linkage has three mobility; whilst, according to the Grübler-Kutzbach's mobility formula, the mobility of this eight-bar linkage is two. Therefore, the directly derivable analysis from screw theory ultimately proves that the proposed eight-bar linkage is an overconstrained spatial linkage.

Synthesis of Fulleroid-like Deployable Platonic Mechanisms

Synthesis and construction of the Fulleroid-like deployable Platonic mechanisms are illustrated in this section through the synthesis and construction of a Fulleroid-like deployable tetrahedral mechanism by implanting a group of the aforementioned eight-bar linkages into a regular tetrahedron base. The method used for synthesizing the Fulleroid-like deployable tetrahedral mechanism can subsequently be extended to the synthesis of the whole group of Fulleroid-like deployable Platonic mechanisms.

Synthesis of A Fulleroid-like Deployable Tetrahedral Mechanism

A regular tetrahedron is shown in Fig. 2 which has four equilateral triangular facets, numbered as f_1, f_2, f_3 and f_4; six edges, denoted by e_1 throughout e_6 that form four vertices A, B, C and D. O_1, O_2, O_3 and O_4 are the centres of the four equilateral triangular facets such that AO_4, BO_1, CO_2 and DO_3 are the normals of faces f_4, f_1, f_2, and f_3, respectively and intersect at point O, i.e. the centroid of the tetrahedron. We use this tetrahedron as a base for synthesizing a Fulleroid-like deployable tetrahedral mechanism. In Fig. 2, the red central lines AO_4, BO_1,
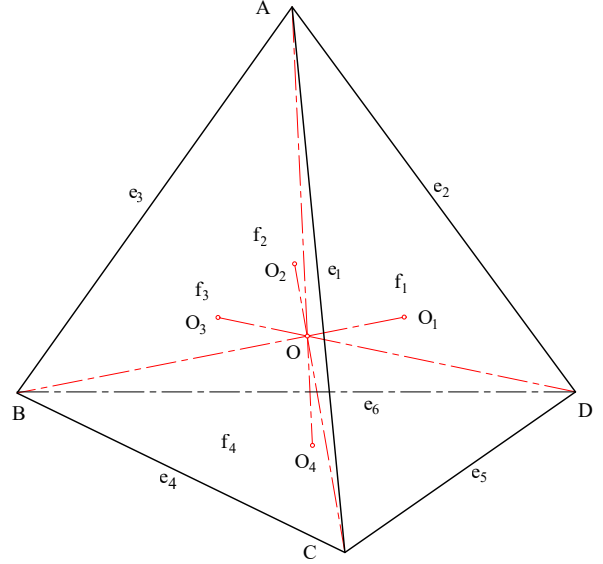

Figure 2. A regular tetrahedron and its geometry

CO_2 and DO_3 are referred to as *virtual axes* and point O is referred to as the *virtual centre* of the mechanism. In the tetrahedron base, as illustrated in Fig. 3a, the proposed overconstrained eight-bar linkage is implanted along the edge e_6 in such an arrangement that all axes of revolute joints A_1, B_1, C_1 and D_1 are perpendicular to facet f_1, and all axes of revolute joints A_2, B_2, C_2 and D_2 are perpendicular to facet f_3. On facet f_1, joints A_1 and B_1 are aligned with CO_1, joints C_1 and D_1 are aligned with AO_1. With regards to facet f_3, joints A_2 and B_2 are aligned with CO_3 while C_2 and D_2 are aligned with AO_3. Referring to Fig. 2, we can calculate the dihedral angle α of a regular tetrahedron as $\alpha_{\text{tet}} = \arccos (1/3)$. In order to build a Fulleroid-like mechanism by using proposed eight-bar linkage, the angle of R-R dyad V-shaped link must meet the requirement of $\varphi_{\text{tet}} = 180° - \alpha_{\text{tet}}$ and lengths of all links in two limbs must be of same value.

Then taking the same procedure we integrate a second identical eight-bar linkage into the tetrahedron base along edge e_5 sharing the same link A_1B_1 with the previous eight-bar linkage, which means link A_3B_3 is as same as link A_1B_1, as shown in Fig. 3b. Axes of joints C_3 and D_3 are perpendicular to facet f_1 and aligned with DO_1, in the meantime, axes of joints A_4, B_4, C_4 and D_4 are perpendicular to facet f_4 with joints A_4 and B_4 lie on CO_4, C_4 and B_4 lie on DO_4.

We then repeat the above procedure three more times by integrating the eight-bar linkages along edges e_2, e_3 and e_4; and by carrying out the detailed structural design, a Fulleroid-like deployable mechanism is constructed as shown in Fig. 4. The mechanism contains five independent loops of the proposed eight-bar linkage with four equilateral triangular facet component labelled as V_1, V_2, V_3 and V_4, and four vertex components denoted as V_A, V_B, V_C and V_D; each facet component connects three identical links whose lengths equal the sides of the facet component itself. The feature of the eight-bar linkage provides the required virtue such that all facet components execute helical motion about their corresponding virtual axes and all
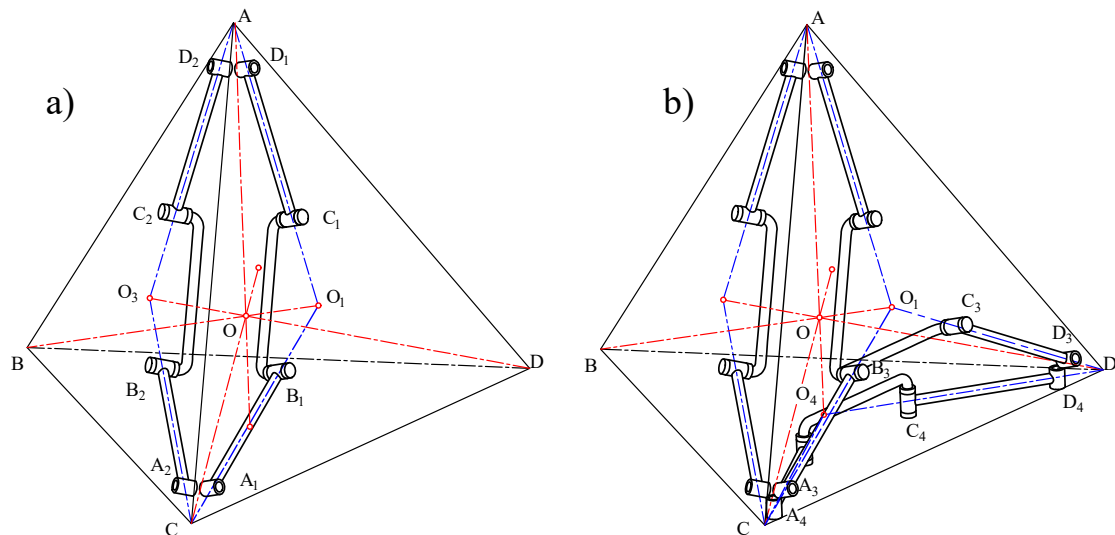
Figure 3. Synthesis of a Fulleroid-like deployable tetrahedral mechanism. Integrate the first and second proposed eight-bar linkage into the tetrahedron base

vertex components will accomplish the radially reciprocating motion, as we expected, along with their corresponding virtual axes towards and outwards the virtual centre O.

As shown in Fig. 4a, in the fully expanded configuration, each vertex reaches the extreme position along the corresponding virtual axes, and in the fully folded configuration, every link overlaps one side of a facet component (Fig. 4c). By taking the very same method, and changing the tetrahedron base to one of the other different bases of Platonic solids, the other deployable mechanisms can be synthesized as well, the detailed discussion is shown in the following subsection.

Number Synthesis and Construction of Fulleroid-like Deployable Platonic Mechanisms

By now, the method for synthesizing a deployable Fulleroid-like tetrahedral mechanism based on proposed overconstrained eight-bar linkage is presented. This method of synthesis can be extended to other bases in the group of Platonic solids. According to Ref.(2), regular polyhedrons such as Platonic polyhedron has the numbers of links and joints that all satisfy the Euler's formula for polyhedrons. Hence, in this section, the numbers of links and joints in the process of synthesizing a Fulleroid-like deployable mechanism is derived and identified.

Considering the properties of the Platonic solids together with the Euler's formula for polyhedrons, the number of links and joints involved in the Platonic mechanisms can be formulated as

$$N_L = v + f + \sum_{i=1}^{f} s_i + \sum_{j=1}^{f} s_j = 3e + 2 \qquad (16)$$

and

$$N_J = 2\sum_{j=1}^{f} s_j = 4e \qquad (17)$$

where N_L and N_J respectively denote the numbers of links and joints embraced in the mechanisms. f, e, v represent

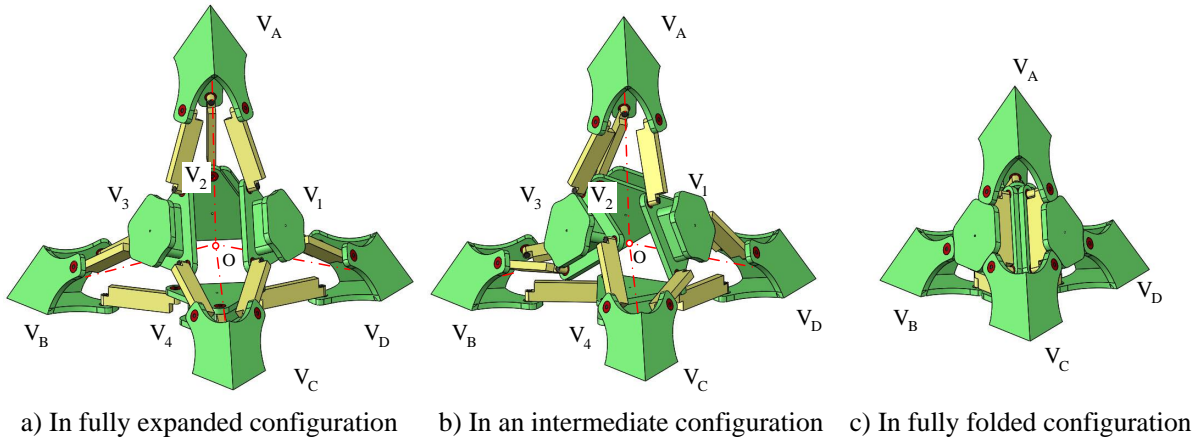**Table 1.** Numbers and structure parameters of the Fulleroid-like deployable Platonic mechanisms

Fulleroid-like deployable Platonic mechanisms	N_L	N_J	α
Tetrahedral mechanism	20	24	109.47°
Hexahedral mechanism	38	48	90°
Octahedral mechanism	38	48	70.53°
Dodecahedral mechanism	92	120	63.43°
Icosahedral mechanism	92	120	41.81°

the numbers of faces, edges, and vertices in the given Platonic polyhedron base, which satisfy the Euler's formula for polyhedrons as $v - e + f = 2$.

Therefore, based on the synthesis method used for the aforementioned Fulleroid-like deployable tetrahedral mechanism, given the structure parameters of the corresponding eight-bar linkages, and link and joint numbers for the corresponding Platonic solid bases in Table 1, the whole group of Fulleroid-like deployable Platonic mechanisms can be synthesized and constructed, and except for the tetrahedral mechanism, Fulleroid-like deployable hexahedral, octahedral, dodecahedral and icosahedral mechanisms are illustrated in Fig. 5.

Mobility and Kinematics of the Fulleroid-like Deployable Platonic Mechanisms

Mobility of the Fulleroid-like deployable Platonic mechanisms can be analysed and verified through the screw-loop equation which is evolved from the mechanical network stemmed from Kirchhoff's circulation law (61). Constraint graphs for the mechanisms are employed leading to constraint matrices of the mechanisms which provide mobility of the mechanisms in every configuration. Further, kinematics of the mechanisms is to be illustrated with numerical simulation as well as prototype.
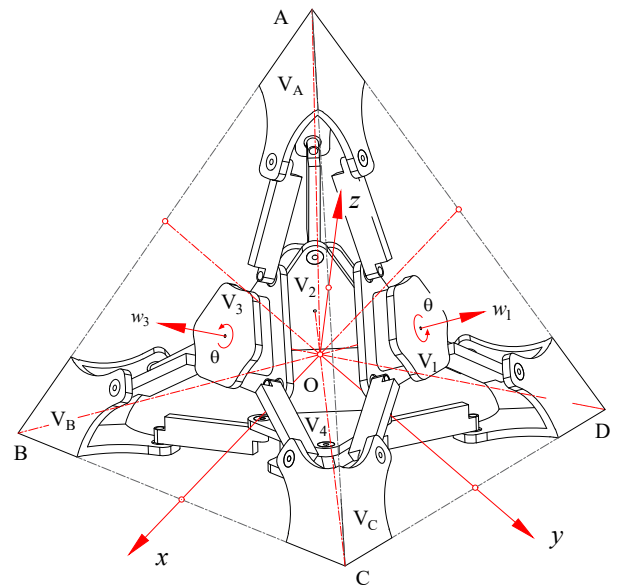
a) In fully expanded configuration b) In an intermediate configuration c) In fully folded configuration

Figure 4. A Fulleroid-like deployable tetrahedral mechanism in different configurations.

a) Hexahedral mechanism   b) Octahedral mechanism

c) Dodecahedral mechanism   d) Icosahedral mechanism
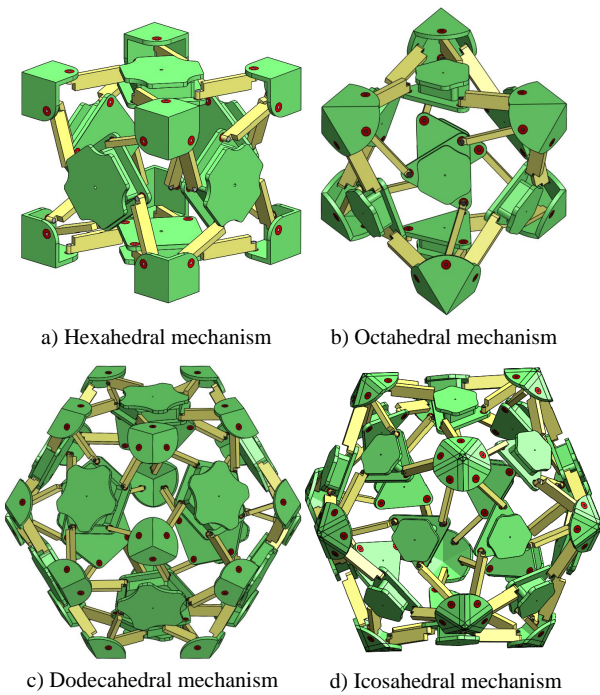
Figure 5. Fulleroid-like deployable Platonic mechanisms

Figure 6. Geometry of deployable Fulleroid-like tetrahedral mechanism

Constraints Matrix and Mobility of the Deployable Fulleroid-like Tetrahedral Mechanism

Mobility analysis of the Platonic mechanism is demonstrated by taking the deployable tetrahedral mechanism as an example. Figure 6 shows an arbitrary configuration of the Fulleroid-like deployable tetrahedral mechanism. A reference coordinate system is established with its origin locating at the virtual centre, and the x-axis passing through the middle points of edges AD and BC, the y-axis passing through the middle points of edges AB and CD, and the z-axis passing through the middle points of edges BD and AC. As can be seen in Fig. 7, in each equilateral triangular facet component, a local coordinate system $\{u_i, v_i, w_i\}$ is attached with its origin O_i locating at the centre of ith facet component ($i = 1, 2, 3, 4$). In the local frame, the w_i-axis is

Figure 7. Joint screws in an individual equilateral triangular facet component

aligned with OO_i, and the u_i-axis is parallel to one of the sides of the equilateral triangular facet.

Lengths of all the links are the same, valued l, the distance between the centre O_i and the axis of the joint connected to the facet component is b, and the distance between O and O_i is d. Since the length of a link equals to length of the side of the facet component, which implies that $b = l/\sqrt{3}$, and according to the geometric relations, there exist $\beta = \arcsin b (\sin\theta / l)$ and $d = l \sin(\theta + \beta) / (2\sqrt{2} \sin\theta)$.

Referring to Fig. 7, joint screws on every individual facet can be calculated with respected to their associated local coordinate system as

$$
\begin{cases}
\boldsymbol{S}_{i1} = \begin{bmatrix} 0 & 0 & 1 & b & 0 & 0 \end{bmatrix}^{\mathrm{T}} \\
\boldsymbol{S}'_{i1} = \begin{bmatrix} 0 & 0 & 1 & b + l\cos\beta & -l\sin\beta & 0 \end{bmatrix}^{\mathrm{T}} \\
\boldsymbol{S}_{i2} = \begin{bmatrix} 0 & 0 & 1 & -\frac{b}{2} & \frac{\sqrt{3}b}{2} & 0 \end{bmatrix}^{\mathrm{T}} \\
\boldsymbol{S}'_{i2} = \begin{bmatrix} 0 & 0 & 1 & -\frac{b + (\cos\beta - \sqrt{3}\sin\beta)l}{2} & \frac{\sqrt{3}b + l(\sqrt{3}\cos\beta + \sin\beta)}{2} & 0 \end{bmatrix}^{\mathrm{T}} \\
\boldsymbol{S}_{i3} = \begin{bmatrix} 0 & 0 & 1 & -\frac{b}{2} & -\frac{\sqrt{3}b}{2} & 0 \end{bmatrix}^{\mathrm{T}} \\
\boldsymbol{S}'_{i3} = \begin{bmatrix} 0 & 0 & 1 & -\frac{b + l(\cos\beta + \sqrt{3}\sin\beta)}{2} & \frac{\sqrt{3}b + l(\sqrt{3}\cos\beta - \sin\beta)}{2} & 0 \end{bmatrix}^{\mathrm{T}}
\end{cases}
\tag{18}
$$

In the above equation, the first subscript $i = 1, 2, 3, 4$ indicting the number of facet component, the joint screws in their local coordinate system of each equilateral triangular individual facet component are able to transformed to the reference coordinate system through an adjoint transformations matrix $\mathbf{A}d_T = \begin{bmatrix} \mathbf{R}_i & \mathbf{0} \\ \tilde{\boldsymbol{p}}_i\mathbf{R}_i & \mathbf{R}_i \end{bmatrix}$ with $\mathbf{R}_i$ being the rotation transformation matrix and $\tilde{\boldsymbol{p}}_i$ being a skew-symmetric matrix derived from $\boldsymbol{p}_i$ which presents the displacements of point O_i in the reference coordinate system. Referring to Fig. 7 with $\boldsymbol{p}_i$, $(i = 1, 2, 3, 4)$ can be calculated and listed in Appendix B. Through the adjoint transformation matrix $\mathbf{A}d_T$, all the joint screws in the tetrahedral mechanism can be obtained with respect to the corresponding local frame system.

According to Euler's formula for independent loop of a mechanical network, the mechanism contains five independent loops such that the constraint graph of the mechanism can be sketched in Fig. 8. According to the constraint graph, the constraint matrix of the Fulleroid-like deployable tetrahedral mechanism is formulated as

$$
\mathbf{M}_c = \begin{bmatrix} \mathbf{M}_{11} & \mathbf{M}_{12} & \mathbf{M}_{13} & \mathbf{0}_{3\times6} \\ \mathbf{M}_{21} & \mathbf{M}_{22} & \mathbf{0}_{2\times6} & \mathbf{M}_{24} \end{bmatrix}
\tag{19}
$$

where the elements $\mathbf{M}_{11}$, $\mathbf{M}_{12}$ and $\mathbf{M}_{13}$ are 3×6 matrices. $\mathbf{M}_{21}$, $\mathbf{M}_{22}$ and $\mathbf{M}_{24}$ are 3×6 matrices. Details for all the matrices can be found in Appendix C. This is a 30×24 matrix and with computer programming, mobility of the mechanism can be determined by the dimension of nullity, i.e., $\dim(N())$, of the constraint matrix $\mathbf{M}_c$ as

$$
\mathrm{M} = \dim(N(\mathbf{M}_c)) = 1
\tag{20}
$$

Above analysis proves that mobility of the Fulleroid-like deployable tetrahedral mechanism is one as we have expected and this is an overconstrained mechanism. Subsequently, mobility of the whole group of Fulleroid-like deployable Platonic mechanisms proposed in this paper can be verified with the same approach.
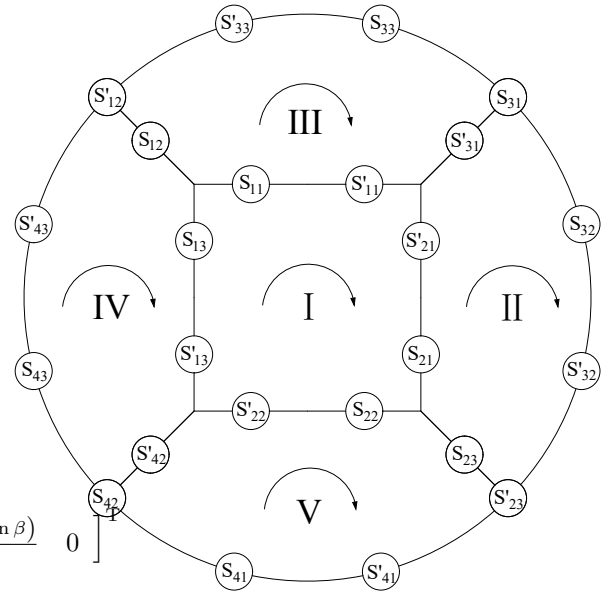

Figure 8. Constraint graph for the tetrahedral mechanism

Kinematics and Motion Simulations of the Fulleroid-like Tetrahedral Mechanism

Since structure of the proposed Sarrus-like eight-bar linkage is similar to the Sarrus linkage, it is expected that given appropriate inputs, the movable platform implements the reciprocating straight-line motion relative to the virtual centre, i.e. point O in Fig. 9. Referring to Fig. 9, we find that one straightforward condition to generate the reciprocating straight-line motion is by given three inputs, e.g., θ_{11}, θ_{21} and θ_{12}, with the two grounded inputs θ_{11} and θ_{21} satisfying $\theta_{11} = \theta_{21}$. In this case, links 3 and 7 in the linkage performs symmetric spatial motion with respect to the plane ACO. However, in order to use this eight-bar linkage to generate Fulleroid-like polyhedral linkages, which requires that links 3 and 7 perform skew-symmetric screw motion, one condition to be satisfied is $\theta_{11} = \theta_{24}$ or $\theta_{14} = \theta_{21}$ and the other kinematic conditions are derived as follows.

Suppose that the movable platform executes reciprocating straight motion, since the structure of the linkage is symmetric to the plane ACO, this implies that the point P must lie on this plane which means the x-component of point P equals 0. The coordinates of point P can be obtained from the fourth columns of $\mathbf{D}_1$ and $\mathbf{D}_2$ in Eqns. (2) and (3) as follows

$$
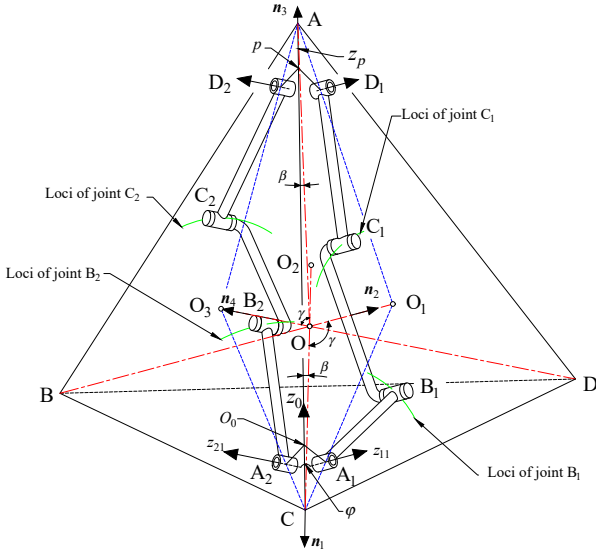x_{P_1} = Aa + Bh = 0
\tag{21}
$$

and

$$
x_{P_2} = A'a + B'h = 0
\tag{22}
$$

with

$$
\begin{aligned}
A &= c(\varphi/2)\left[c\theta_{11} + c(\theta_{11} + \theta_{12}) + c(\theta_{11} + \theta_{12} + \theta_{13})\right] \\
B &= c(\varphi/2)\left[1 + c(\theta_{11} + \theta_{12} + \theta_{13} + \theta_{14})\right] \\
A' &= c(\varphi/2)\left[c\theta_{21} + c(\theta_{21} + \theta_{22}) + c(\theta_{21} + \theta_{22} + \theta_{23})\right] \\
B' &= c(\varphi/2)\left[1 + c(\theta_{21} + \theta_{22} + \theta_{23} + \theta_{24})\right]
\end{aligned}
$$

hereafter, s and c in equations respectively stand for the sine and cosine functions.

Since a, h are parameters related to link length, φ is less than 180 deg. From Eqns. (21) and (22) there must be $A = 0$,

Figure 9. An eight-bar linkage in a regular tetrahedral base

$B = 0$, $A' = 0$ and $B' = 0$, which leads to the following equations

$$\begin{cases} c\theta_{11} + c(\theta_{11} + \theta_{12}) + c(\theta_{11} + \theta_{12} + \theta_{13}) = 0 \\ \theta_{11} + \theta_{12} + \theta_{13} + \theta_{14} = \pi \end{cases} \quad (23)$$

and

$$\begin{cases} c\theta_{21} + c(\theta_{21} + \theta_{22}) + c(\theta_{21} + \theta_{22} + \theta_{23}) = 0 \\ \theta_{21} + \theta_{22} + \theta_{23} + \theta_{24} = \pi \end{cases} \quad (24)$$

Further, the movement of the movable platform can be presented by the point P in limb 1 and limb 2 as

$$\boldsymbol{p_1} = \begin{bmatrix} x_p \\ y_p \\ z_p \end{bmatrix} = \begin{bmatrix} 0 \\ 0 \\ a\left[s\theta_{11} + s(\theta_{11} + \theta_{12}) + s(\theta_{11} + \theta_{12} + \theta_{13})\right] \end{bmatrix} \quad (25)$$

and

$$\boldsymbol{p_2} = \begin{bmatrix} x_p \\ y_p \\ z_p \end{bmatrix} = \begin{bmatrix} 0 \\ 0 \\ a\left[s\theta_{21} + s(\theta_{21} + \theta_{22}) + s(\theta_{21} + \theta_{22} + \theta_{23})\right] \end{bmatrix} \quad (26)$$

which implies that the movement of platform is only along the direction of z-axis in reference coordinate system, i.e., it executes an exact straight line motion. Hence, each limb of the proposed eight-bar linkage has one extra revolute joint together with an extra link compared to Sarrus linkage.

By recalling Section , as can be seen in Fig.9, it is found that if the joint angles comply with $\theta_{11} = \theta_{24}$, $\theta_{12} = \theta_{23}$ and $\theta_{13} = \theta_{22}$, the link B_1C_1 and B_2C_2 which make a contributions to form equilateral triangular facet component will do a screw motion about OO_1 and OO_3, respectively. Link A_1A_2 and D_1D_2 respectively execute radially reciprocating motion along CO and AO. Therefore, the angles bewteen line OO_1 and CO, OO_3 and OA are the same, denoted as γ. In Fig.9, dashlines OC and OA are represented by normals $\boldsymbol{n_1}$ and $\boldsymbol{n_3}$, respectively. Dashlines OO_1 and OO_3 are represented by normals $\boldsymbol{n_2}$ and $\boldsymbol{n_4}$, reprectively. Therefore, there exists

$$\boldsymbol{n_1}^T \boldsymbol{n_2} = \boldsymbol{n_3}^T \boldsymbol{n_4} \quad (27)$$

where $\boldsymbol{n_1}$, $\boldsymbol{n_2}$ can be calculated by referring to Figs.1 and 9 as

$$\boldsymbol{n_1} = \begin{bmatrix} 1 & 0 & 0 \\ 0 & \cos(-\beta) & -\sin(-\beta) \\ 0 & \sin(-\beta) & \cos(-\beta) \end{bmatrix} \begin{bmatrix} 0 \\ 0 \\ -1 \end{bmatrix} = \begin{bmatrix} 0 \\ -\sin\beta \\ -\cos\beta \end{bmatrix} \quad (28)$$

and

$$\boldsymbol{n_3} = \begin{bmatrix} 1 & 0 & 0 \\ 0 & \cos\beta & -\sin\beta \\ 0 & \sin\beta & \cos\beta \end{bmatrix} \begin{bmatrix} 0 \\ 0 \\ 1 \end{bmatrix} = \begin{bmatrix} 0 \\ -\sin\beta \\ \cos\beta \end{bmatrix} \quad (29)$$

Normals $\boldsymbol{n_2}$ and $\boldsymbol{n_4}$ can be extracted from the third columns of the homogeneous coordinates of joints B_1 and B_2, respectively, which are being expressed as

$$\boldsymbol{n_2} = \begin{bmatrix} \sin\left(\frac{\varphi}{2}\right) & -\cos\left(\frac{\varphi}{2}\right) & 0 \end{bmatrix}^T \quad (30)$$

and

$$\boldsymbol{n_4} = \begin{bmatrix} -\sin\left(\frac{\varphi}{2}\right) & -\cos\left(\frac{\varphi}{2}\right) & 0 \end{bmatrix}^T \quad (31)$$

Hence, equation (27) yields the result that $\boldsymbol{n_1}^T \boldsymbol{n_2} = \boldsymbol{n_3}^T \boldsymbol{n_4} = \sin\beta\cos\left(\frac{\varphi}{2}\right) = \cos\gamma$ which means once the eight-bar linkage is embedded in a tetrahedron base, the angle γ is a structure parameter, given a Platonic polyhedron base, the angles β and φ are determined. In this case, $\varphi = \pi - \arccos(1/3) = 109.47°$.

From Eqns. (25) and (26), we have

$$\sin\theta_{11} + \sin(\theta_{11}+\theta_{12}) + \sin(\theta_{11}+\theta_{12}+\theta_{13}) = \\ \sin\theta_{21} + \sin(\theta_{21}+\theta_{22}) + \sin(\theta_{21}+\theta_{22}+\theta_{23}) \quad (32)$$

combining Eqn. (32) with the Eqns. (23) and (24), it yields

$$s\theta_{11} + s(\theta_{13}+\theta_{14}) + s\theta_{14} = s\theta_{21} + s(\theta_{21}+\theta_{22}) + s\theta_{24} \quad (33)$$

Further, considering the condition $\theta_{11} = \theta_{24}$, Eqn. (33) can be rewritten as

$$\sin(\theta_{13}+\theta_{14}) + \sin\theta_{14} = \sin\theta_{21} + \sin(\theta_{21}+\theta_{22}) \quad (34)$$

Referring Figs. 3 and 4, assuming that $\theta_{21} = \theta_{14}$, we have

$$\sin(\theta_{13}+\theta_{14}) = \sin(\theta_{21}+\theta_{22}) \quad (35)$$

which means $\theta_{11} + \theta_{12} = \theta_{23} + \theta_{24}$ that implies $\theta_{12} = \theta_{23}$ and $\theta_{13} = \theta_{22}$.

So far, it is found that if the joints angle comply with $\theta_{11} = \theta_{24}$, $\theta_{12} = \theta_{23}$ and $\theta_{13} = \theta_{22}$ and given three skew-symmetric inputs, the point P located in the movable platform will executes an exact straight-line motion along the edges of tetrahedron base, e.g., edge AC, as illustrated in Fig. 9. In this condition, the four joints B_1, C_1, B_2, C_2 plot the helical curves which implied that each pair of them forms a double helix. Inspired by the feature of linkage which is able to carry out double helix motion, it is found that by properly implanting this presented overconstrained eight-bar linkage into a group of Platonic polyhedron bases and combining with the characterization of Fulleroid-like mechanism, a group of deployable Fulleroid-like Platonic mechanisms can be well-synthesized and constructed.
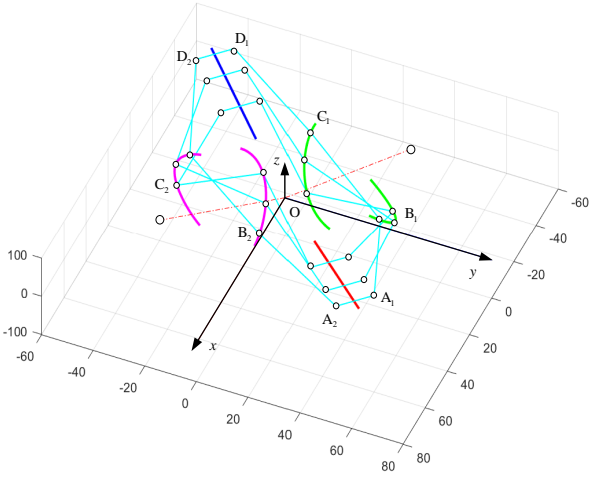
Figure 10. Motion simulation for the eight-bar linkage

Figure 11. Motion of the deployable Fulleroid-like tetrahedral mechanism

Simulation by programming for motion analysis of the eight-bar linkage in a regular tetrahedral base is shown in Fig. 10 as a verification compared to Fig. 9. For link B_1C_1, traces of points B_1 and C_1 draw a double helix and so do the points B_2 and C_2, form another double helix. This clearly shows that the equilateral triangular facet components (link 3 and link 7 of the proposed eight-bar linkage) perform screw motions about their corresponding virtual axes (OO_1 and OO_3) and the vertex components (link 1 and link 5 composed of joints A_1, A_2 and D_1, D_2) execute radially reciprocating motions along their associated virtual axes towards or outwards the virtual centres.

This simulation verifies that the proposed eight-bar linkage can achieve the motion as expected. By extending the motion simulation to the deployable Fulleroid-like tetrahedral mechanism, the motion performance shown in Fig. 11. The figure indicates that in the deployable tetrahedral mechanism the four facet components carry out screw motions about their associate virtual axes and four vertex components perform radially reciprocating motions along their corresponding virtual axes towards and outwards the virtual centre O. By using the similar approach, kinematics of the whole group of Fulleroid-like Platonic mechanisms can be investigated and analyzed.

With the proof of well-implemented radially reciprocating motion of the four vertices and four triangular facet components, the relationship between these two velocities (vertex and triangular facet component along their vertical axes respectively) and angle θ (degree) of the actuated triangular facet component is revealed as follows.

According to the geometry of deployable Fulleroid-like tetrahedral mechanism in Figs. 6 and 7, there exists
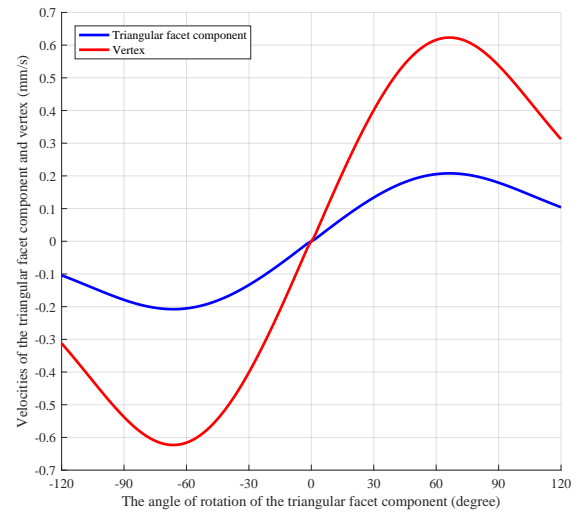
$$\begin{cases} \beta\left(I\right) = \arcsin\left[b\sin\left(\theta\left(I\right)\right)/l\right] \\ d\left(I\right) = l\sin\left[\theta\left(I\right) + \beta\left(I\right)\right]/\left[2\sqrt{2}\sin\left(\theta\left(I\right)\right)\right] \end{cases} \quad (36)$$

where I is the angle of actuated component in the range of $I \in [-120°, 120°]$, and the angular velocity is one degree per second. The displacement increment of d along its virtual axis in the I*th* second is

$$\Delta d\left(I\right) = d\left(I\right) - d\left(I-1\right) \quad (37)$$
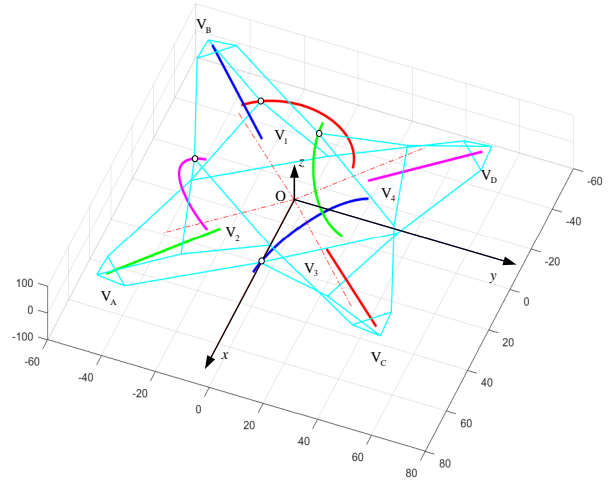
Figure 12. Velocities of triangular facet component along their virtual axes

and the displacement increment of vertex along its virtual axis denoted by $\Delta d_V\left(I\right)$ in the I*th* second is

$$\Delta d_V\left(I\right) = 3\left[d\left(I\right) - d\left(I-1\right)\right] = 3\Delta d\left(I\right) \quad (38)$$

Hence in each particular second, the velocities of the triangular facet component and vertex can be expressed as $\upsilon\left(I\right) = \Delta d\left(I\right)$ and $\upsilon_V\left(I\right) = \Delta d_V\left(I\right)$. With the parameters of $l = 50$mm and $b = 28.868$mm, by programming in Matlab®, the velocities of triangular facet component and vertex along their virtual axes in a specified actuated angle is illustrated in Fig. 12. It shows the folding process from fully-expanded configuration to fully-folded configuration followed by the process of expanding from fully-folded configuration to fully-expanding configuration.

An Application of the Deployable Fulleroid-like Hexahedral Mechanism and Its Prototype

All the investigations and the simulations of the synthesized Fulleroid-like tetrahedral mechanism indicates that the

presented eight-bar linkage has a good adaptability for synthesizing others Platonic solids. In section , all of the five synthesized deployable Fulleroid-like Platonic mechanisms are introduced. In each mechanism, with the acknowledgement of the link length is equal to the side length of each facet component, assuming that the number of sides for a facet component is s, expansion ration r_e of the mechanism defined and calculated by ratio of the volumes of changed mechanisms (from fully-expanded to fully-folded configurations), can be formulated as

$$r_e = 8\left(\cos\frac{\pi}{s}\right)^3 \tag{39}$$

which means that the expansion ratio of the tetrahedral mechanism approximately is 8. Therefore, the deigners should exploit this feature in developing robotic structures.

In this section, the authors choose the hexahedron as another ideal base for synthesizing (see Fig. 5a) a deployable Fulleroid-like mechanism. The vertex of the synthesized deployable Fulleroid-like hexahedral mechanism is replaced with a spherical-surface vertex. This is an adapting application and the whole mechanism can be transformed into a sphere cell from the fully-expanded configuration. Transforming process from fully-expanded to fully-folded configurations is illustrated in Fig. 13. Based on the implementation of these designed structures and functions, the deployable spherical hexahedral mechanism is treated as a deployable carrier which can be used to store sensing system, micro crawling/wheeled robots and other related apparatuses. It is known that all the five deployable Platonic mechanisms turn out to be highly overconstrained mechanisms with one mobility, so in the deployable spherical hexahedral carrier, with the help of certain device (like servo motor) to control the rotation of either one link, the carrier could be expanding. When the servo motor rotates and retains in certain positions, this carrier will be locked and held still in a series of configurations.

The prototype of the deployable Fulleroid-like spherical hexahedral mechanism can be constructed and properly assembled through 3D printing method as illustrated in Fig. 13. Testing this prototype by manually driven, rotating either one of the links a certain angle, it indicates that the presented deployable Fulleroid-like spherical hexahedral mechanism has one mobility and all the six square facet components perform screw motion about their corresponding virtual axes and the eight sphere vertex components execute reciprocating motions along their associated virtual axes towards or outwards the virtual centre.

Further, by integrating the spherical hexahedral mechanism with a reconfigurable rotor frame as illustrated in Fig. 14, a deployable quadrotor was designed and developed. This quadrotor has variable configurations associated with variable rotor lever length. The deployable mechanism provides augmented storage space and the reconfigurable structure provides diverse configurations to be selected for different specified tasks/missions.

Finite Element Analysis of the Proposed Deployable Quadcopter

Strength and stability of the reconfigurable rotor-arm system are critical parameters to ensure the manoeuvrability of the
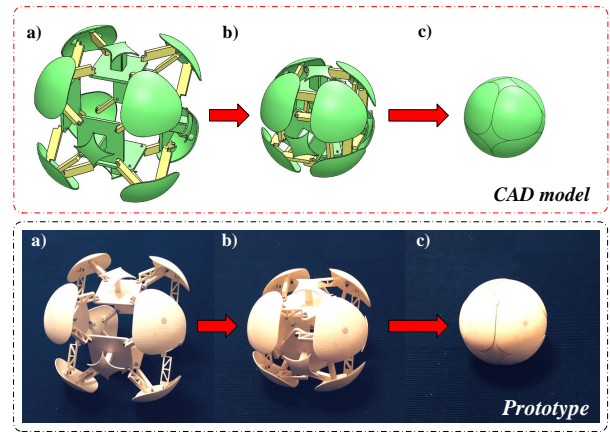

Figure 13. The CAD model and prototype of a deployable Fulleroid-like spherical hexahedral mechanism. a) in the fully-expanded configuration. b)in an intermediate configuration. c)in the fully-folded configuration.

quadcopter. As pointed out by Mintchev(62), if the arms are too flexible, they could bend and vibrate during flight leading to instability and reducing the quadcopters reaction time to the external comments. Hence, in the section structure of the proposed reconfigurable quadcopter is analysed using FEA method. The quadcopter is mainly fabricated by 3D printing method and assembled with aluminium alloy link connected with sliding rod and circular plate in reconfigurable rotor frame. Material parameters of ABS and aluminium are derived from the material library of SolidsWorks®.

The finite element models under two typical working situations (one is in an intermediate configuration and another is in fully expanded configuration) are selected for static structural analysis. The analysis and simulations are achieved in ANSYS® Workbench 17.0 environment. Considering gravity and applying thrust of 10N each to the four rotors of the quadcopter, the deformations and stress of two different configurations are shown in Fig. 15, which indicates that the maximum displacement with a peak value of 0.12849mm occurs at the edge of each arm where the motor was mounted, in the fully expanded configuration. Figure 15 also shows that the maximum stress with a value of 18.245Mpa occurs at the links which connected with the vertices and square facet components. The equivalent stress details of these rotor-arm, square facet component and link component are shown in Figs. 16 and 17.

For the stress in rotor arm structure indicated in Fig. 16, in both of the two configurations, stress is mainly distributed along the rod in which connected with the square facet component with the value of around 5Mpa. The maximum stress in rotor arm structure occurs at the tail end near the small hole for the small link pull through to connect to the circle plate. The peak value of this stress is 11.094Mpa in the intermediate configuration which is 0.536Mpa bigger than in fully expanded configuration. For the calculated stress shown in square facet component in each configuration, the difference of maximum values is significantly increased which is 4.132Mpa. The maximum stress happened at the link among all components in two configurations with slightly different peak value. In the fully expanded configuration, maximum stress happened at
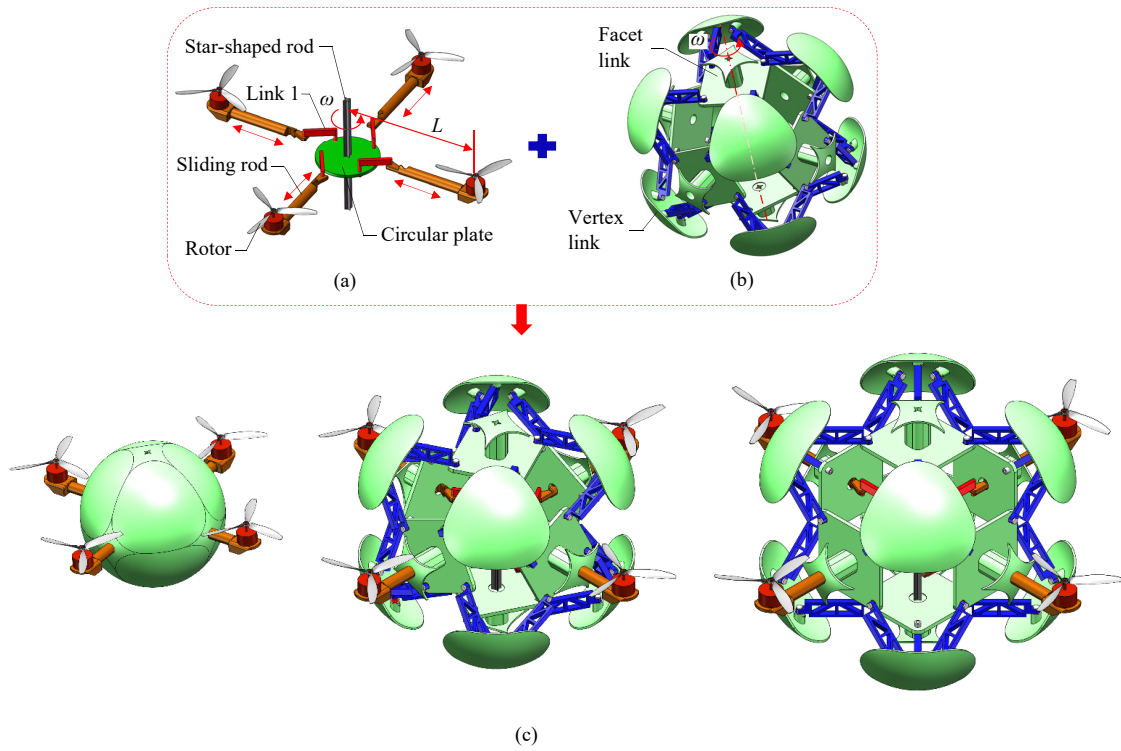
Figure 14. A deployable quadrotor. (a) A reconfigurable rotor frame and the rotors. (b) A deployable hexahedral mechanism. (c) Three typical configurations of the deployable quadrotor.
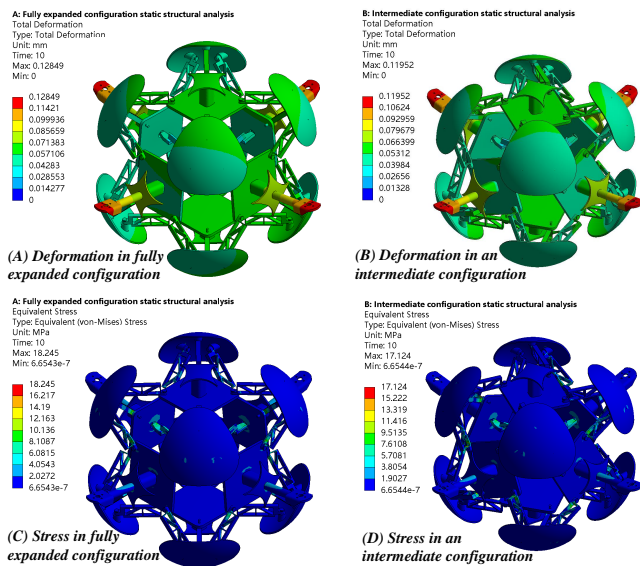
**Figure 15.** Deformations and stress of the deployable quadcopter in two configurations
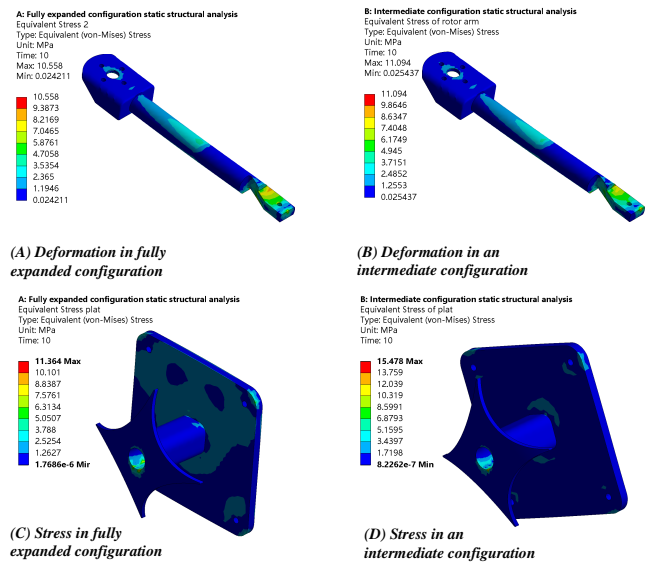
Figure 16. Stress of rotor-arm structure and square facet component in two configurations

the link-24 as can be seen in Fig. 17(A) with the value of 18.245Mpa. But it changes to link-22 when it is in an intermediate configuration, v alued 1 7.12Mpa (see Fig. 17(B)). The stress discussed in this part is less than 20Mpa which means the ABS material is strong enough for supply the thrust generated for lifting the quadcopter.

Dynamic Modelling and Simulation of the Proposed Deployable Quadcopter

Dynamic modelling of the deployable quadrotor is presented in (63). In order to carry out numerical simulation based on the mathematical model established, mass and moment of inertia of the quadrotor and the rotors are obtained from the CAD model of the proposed quadrotor. Then by converting the above mathematical model into Simulink® model, and substituting the structure parameters, numerical simulation of the proposed quadrotor is conducted in this section. In

(A)Fully expanded configuration

(B)Intermediate configuration
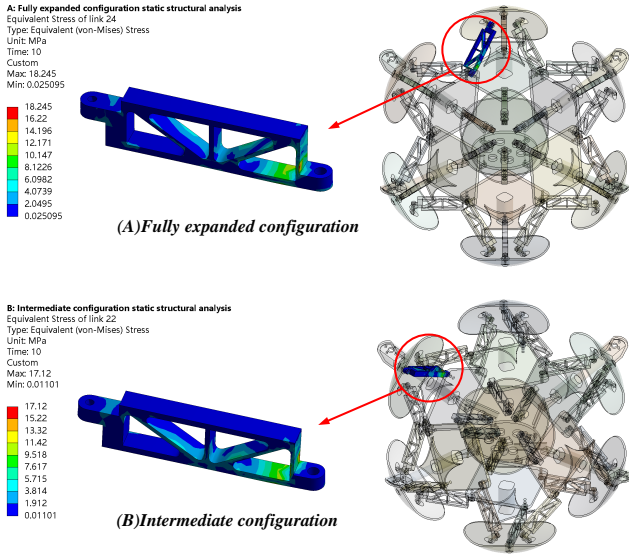
Figure 17. (A)Maximum stress occured at link-24 in fully expanded configuration (B) Maximum stress occured at link-22 in an intermediate configuration

Figure 18. The control inputs ω_i

Figure 19. Positions x, y and z of the quadcopter in fully folded configuration

Figure 20. Angles ϕ, θ, and ψ of the quadcopter in fully folded configuration

order to determine the thrust for lifting the quadrotor in windless environment, the angular velocities of the four rotors need to be equal. The quadrotor ascends when all of the four rotors are accelerated.

Four inputs U_1, U_2, U_3, U_4 defined as

$$
\begin{bmatrix} U_1 \\ U_2 \\ U_3 \\ U_4 \end{bmatrix} = \begin{bmatrix} k \sum \omega_i{}^2 \\ k(\omega_2{}^2 - \omega_1{}^2) \\ k(\omega_3{}^2 - \omega_4{}^2) \\ b(\omega_1{}^2 + \omega_2{}^2 - \omega_3{}^2 - \omega_4{}^2) \end{bmatrix} \tag{40}
$$

are used to control the lift, roll, pitch and yaw motion of the quadrotor.

The simulation starts with the configuration when the deployable hexahedral mechanism is fully folded. Then influence of the reconfiguration of the deployable hexahedral mechanism, which causes changes to the lever length L and moment of inertia J_{xx}, J_{yy}, J_{zz} on the dynamic performance is simulated and compared. The parameters used in the simulation are listed in Table 2. The values of the drag force coefficients k_x, k_y and k_z are assigned such that the quadrotor will slow down and stop when the angles ϕ and θ are stabilized to zero values.

In the simulation, the quadrotor is assumed to be initially in a stable state in which the values of positions and angles are zero, the body frame of quadrotor is congruent with the inertial frame. In order to determine the total thrust for the take-off of quadrotor in windless environment, the angular velocities of the four rotors need to be equal. The quadcopter ascends when all of the four rotors are accelerated. At this moment, the total thrust is equal to the hover thrust. The simulation is processed at 0.000001 second intervals to total elapsed time of 2 seconds. The control inputs, the angular velocities of the four rotors are indicated in Fig. 18.
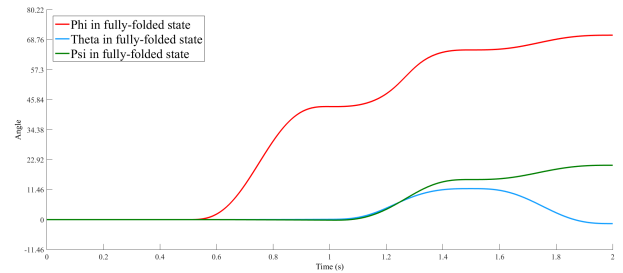
For the case when the deployable hexahedral mechanism is in fully folded configuration, the inertial position x, y and z and orientation, i.e. angles ϕ, θ and ψ are shown in Fig. 19 and Fig. 20
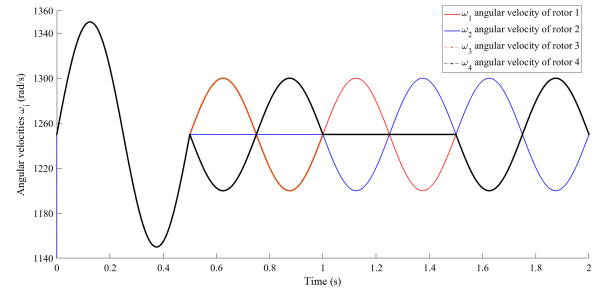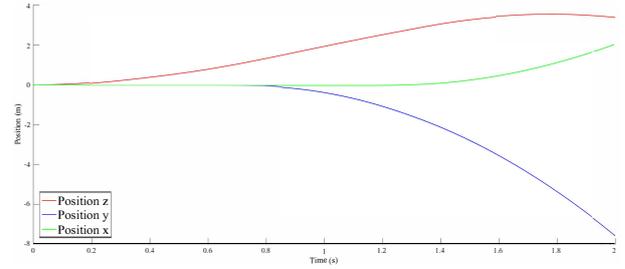
For the first 0.25 seconds, the quadrotor ascended by giving all of the rotor velocities from the hover thrust as mentioned previously which is 1250 rad/s, then the ascend is gradually reduced by decreasing the rotor velocities significantly for the following 0.25 seconds, as can be seen in Fig. 18. Consequently, the quadrotor ascended 0.6 meters in the first 0.5 seconds.

After finished the 0.5 seconds of lifting motion the quadrotor is stable again and ready for performing roll motion by increasing the velocity of the third rotor and decreasing the velocity of the fourth rotor for 0.25 seconds. Then, the acceleration of the roll motion is stopped bu decreasing the velocity of the third rotor and increasing the velocity of the fourth rotor. Thus, after 0.5 seconds of rolling, the roll angle ϕ had increased approximately 43.2 degrees, seeing in Fig. 20, the rolling motion started from 0.5 seconds and there is no sign of any pitch motion nor yaw motion in this period.

Then, similar to the roll motion, the quadrotor is put into a pitch motion by increasing the velocity of the first rotor and decreasing the velocity of the second rotor for 0.25 seconds. The pitch motion is stopped by decreasing the velocity of the first rotor and increasing the velocity of the second rotor. After this period of pitch movement, the pitch angle θ had increased approximately 11.2 degrees, seeing in Fig. 20.

Table 2. Parameter values of dynamic simulation

Statements	m (kg)	L (m)	$k_x = k_y = k_z$ (kg/s)	J_{xx} (kg·m²)	J_{yy} (kg·m²)	J_{zz} (kg·m²)	J_r (kg·m²)	k	b
Fully-expanded	1.33	0.230	0.25	1.833e-2	2.231e-2	1.833e-2	3.357e-5	2.98e-6	1.14e-7
Intermediate	1.33	0.215	0.25	1.616e-2	1.958e-2	1.616e-2	3.357e-5	2.98e-6	1.14e-7
Fully-folded	1.33	0.159	0.25	5.867e-3	7.602e-3	5.867e-3	3,357e-5	2.98e-6	1.14e-7
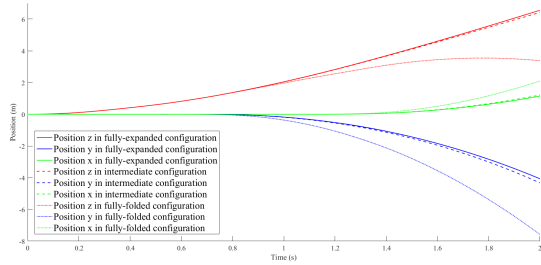
Figure 21. Positions x, y and z of the quadcopter in three configurations
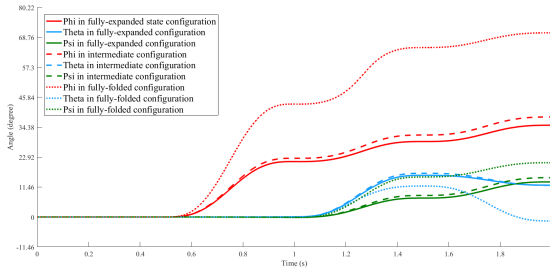
Figure 22. Angles ϕ, θ, and ψ of the quadcopter in three configurations

Finally, the quadrotor is turned in the direction of the yaw angle ψ by increasing the velocities of the second and the first rotors and decreasing the velocities of the fourth and the third rotors simultaneously for 0.25 seconds and after this, decreasing the velocities of the second and the first rotor and increasing the velocities of the fourth and the third rotors at the same time for the last 0.25 seconds. As can be seen in Fig. 20, consequently the yaw angle ψ had increased approximately 20.78 degrees.

We run the simulation another two times for representing three different configurations of the deployable quadrotor, fully folded statement, fully expanded statement and a random intermediate statement, respectively. It has been known that the reconfigurable mechanism causes changes length between the rotor and the center of mass of the whole model as well as the moments of inertia. Hence, it makes senses to compare the simulation results of each statement. Based on the parameter values of dynamic simulation, the results of three different configurations are illustrated in Figs. 21 and 22.

Results show that they had the same changing trend but due to the high expansion ratio of the deployable hexahedral mechanism as introduced in Fig. 14, the values of moments of inertia of the quadrotor varies significantly. This markedly appears in angle curves in Fig. 22, when the quadrotor is put into a rolling movement, roll angle ϕ of fully folded configuration is 2.25 times more likely to the fully expanded configuration which is 28.48 degrees. There is another

point worth noticing that different configurations may cause positions varied. In Fig. 21, at the end of simulations, the positions of x, y and z showed a relatively big change compared to the other configurations. This indicates that the maneuverability and stability of this quadrotor are getting challenging with dwindling in size of the quadrotor, which requires a better control strategy.

Conclusions

In this paper, a new overconstrained spatial eight-bar linkage with mobility of three was proposed and applied to the synthesis of a group of Fulleroid-like deployable Platonic polyhedral mechanisms. Structure of the proposed eight-bar linkage was introduced including geometric information and structure equation of the closed-loop linkage. Subsequently, the mobility of the linkage was identified by using screw theory. Further, choosing tetrahedron as an example, process of synthesizing a deployable Fulleroid-like tetrahedral mechanism was presented and illustrated providing a straightforward and geometrically intuitive method for synthesis of the group of Fulleroid-like deployable Platonic mechanisms. Then, mobility of the deployable mechanism was formulated and verified based on Kirchhoff's circulation law for mechanical networks (by drawing constraint graph) leading to the constraint matrix which determines the mobility. Moreover, kinematics of the eight-bar linkage and the deployable Platonic mechanisms were analysed and illustrated with numerical simulations shedding lights on motion characteristics of the eight-bar linkage and the synthesized polyhedral mechanisms. It is demonstrated that the overconstrained eight-bar linkage is capable of generating double-helix motion integrated with straight-line motion. Moreover, for all the other Fulleroid-like deployable Platonic mechanisms presented in this paper, no matter the equilateral triangular facet component in deployable tetrahedral and octahedral and icosahedral mechanisms, or the square facet component in deployable cube mechanism, or the pentagonal facet component in deployable dodecahedral mechanism, they all perform screw motions about their corresponding virtual axes and the vertex components execute radially reciprocating motions along their associated virtual axes towards or outwards the virtual centres.

An adapting application based on the deployable Fulleroid-like hexahedral mechanism was designed by replacing vertex with a sphere surface vertex so that the mechanism could be able to fold into a cell. The design can be used as a deployable carrier for developing and improving existing robotic structures thanks to the high expansion ratio of the mechanism. The carrier can load sensing system or equip micro crawling devices/wheels. A prototype of the proposed deployable carrier was built through 3D

printing technology. In addition, the proposed deployable hexahedral mechanism was applied in the development of a reconfigurable quadrotor with static structural analyses and dynamic simulations being carried out. Control of such a novel quadrotor will be target for our further research and we expect that this research will embark on the relevant research that merges deployable mechanisms with the development of UAV technology. The PID control and development of prototype of the proposed deployable quadrotor are under conduct and will be presented in the future research papers.

Acknowledgements

References

[1] Bennett GT. The skew isogram mechanism. In *Proceedings of the London Mathematical Society*. pp. 151–173.

[2] Wei G, Chen Y and Dai JS. Synthesis, mobility and multifurcation of deployable polyhedral mechanisms with radially reciprocating motion. *Transactions of the ASME: Journal of Mechanical Design* 2014; 136(11).

[3] McCarthy JM. *An Introduction to Theoretical Kinematics*. MIT Press, 1990.

[4] Wittenburg J. *Kinematics: Theory and Applications*. Berlin, Heidelberg: Springer, 2016.

[5] Sarrus PF. Note sur la transformation des mouvements rectilignes alternatifs, en mouvements circulaires; et reciproquement. *Academie des Sciences* 1853; 36: 1036–1038.

[6] Goldberg M. New five-bar and six-bar linkages in three dimensions. *Transactions of the ASME* 1943; 65: 649–661.

[7] Myard FE. Contribution à la géométrie des systèmes articulés. *Bulletin de la Socit Mathmatique de France* 1931; 59: 183–210.

[8] Myard FE. Sur les chaines fermées à quatre couples rotoïdes non-concourants, deformables au premier degré de liberté isogramme torique. *Compterendus de l'Acadèmie de Science* 1931; 192: 1194–1196.

[9] Bricard R. *Leçons de cinématique*. Paris, France: Gauthier-Villars, 1926.

[10] KJWaldron. Hybrid overconstrained linkages. *Journal of Mechanisms* 1968; 3(2): 73–78.

[11] Schatz P. *Rhythmusforschung und Technik*. Stuttgart, Germany: Freies Geistesleben, 1975.

[12] Wohlhart K. A new 6R space mechanism. In *Proc. 7th IFToMM World Congress*, volume 1. pp. 193–198.

[13] Wohlhart K. Merging two general goldberg 5R linkages to obtain a new 6R space mechanism. *Mechanism and Machine Theory* 1991; 26: 659–668.

[14] Baker JE. A comparative survey of the bennett-based, 6-R revolute kinematic loops. *Mechanism Machine Theory* 1993; 28: 83–96.

[15] Mavroidis C and Roth B. Analysis and synthesis of overconstrained mechanisms. *Transactions of the ASME: Journal of Mechanical Design* 1995; 117: 75–82.

[16] Baker JE. Overconstrained six-bars with parallel adjacent joint-axes. *Mechanism and Machine Theory* 2003; 38(2): 103–117.

[17] Chen Y and You Z. An extended myard linkage and its derived 6R linkage. *Journal of Mechanical Design* 2008; 130(10): 052301.

[18] Cui L and Dai JS. Axis constraint analysis and its resultant 6R double-centered overconstrained mechanisms. *Journal of Mechanisms and Robotics* 2011; 3(3): 031004.

[19] Dietmaier P. *Einfach übergeschlossene Mechanismen mit Drehgelenken*. Habilitation thesis, Graz University of Technology, 1995.

[20] Chen Y and You Z. On mobile assemblies of bennett linkages. In *Proceedings of the Royal Society of London A: Mathematical, Physical and Engineering Sciences*. pp. 1275–1293.

[21] Qi XZ, Deng ZQ, Ma BY et al. Design of large deployable networks constructed by myard linkages. *Key Engineering Materials* 2011; 486: 291–296.

[22] Huang H, Deng Z and Li B. Mobile assemblies of large deployable mechanisms. *Journal of Space Engineering* 2012; 5(1): 1–14.

[23] Kiper G and Söylemez E. Regular polygonal and regular spherical polyhedral linkages comprising bennett loops. In *Computational Kinematics: Proceedings of the 5th International Workshop on Computational Kinematics*. pp. 249–256.

[24] Verheyen HF. Expandable polyhedral structures based on dipolygonids. In *Proc. 3rd Int. conf. Space Structures*. London, UK: Elsevier.

[25] Verheyen HF. The complete set of jitterbug transformers and the analysis of their motion. *Computers & Mathematics with Applications* 1989; 17(1-3): 203–250.

[26] Wohlhart K. Heureka octahedron and brussels folding cube as special cases of the turning tower. In *Proc. the Sixth IFToMM International Symposium on Linkages and Computer Aided Design Methods*. Bucharest, Romania.

[27] Wohlhart K. New overconstrained spheroidal linkages. In *Proc. the Ninth World Congress on the Theory of Machines and Mechanisms*. Milano, Italy.

[28] Wohlhart K. Kinematics and dynamics of the fulleroid. *Multibody Systems Dynamies* 1997; 1: 241–258.

[29] Wohlhart K. Kinematics of röschel polyhedra. In Lenarčič J and Husty M (eds.) *Advances in Robot Kinematics: Analysis and Control*. Kluwer Akademie Publisher, 1998.

[30] Wohlhart K. Deformable cages. In *10th World Congress on the Theory of Machines and Mechanisms*. Oulo, Finland, pp. 683–688.

[31] Wohlhart K. Double-ring polyhedral linkages. In *Proc. Interdisciplinary Applications of Kinematics*. Peru, Lima.

[32] Wohlhart K. New polyhedral star linkages. In *Proc. the 10th International Conference on the Theory of Machines and Mechanisms*. Liberec, Czech Republic.

[33] Wohlhart K. Polyhedral zig-zag linkages. In *On Advances in Robot Kinematics*. Dordrecht, Netherlands.

[34] Agrawal SK, Kumar S and Yim M. Polyhedral single degree-of freedom expanding structures: design and prototypes. *Transactions of the ASME: Journal of Mechanical Design* 2002; 124(9): 473–478.

[35] Chen Y, Guest SD, Fowler P et al. Two-orbit switch-pitch structures. *Journal of the International Association for Shell and Spatial Structures* 2012; 53: 157–162.

[36] Chen Y, Feng J and Liu Y. A group-theoretic approach to the mobility and kinematic of symmetric over-constrained structures. *Mechanism and Machine Theory* 2016; 105: 91 – 107.

[37] Chen Y, Fan L and Feng J. Kinematic of symmetric deployable scissor-hinge structures with integral mechanism mode. *Computers & Structures* 2017; 191: 140 – 152.

[38] Gosselin CM and Gagnon-Lachance D. Expandable polyhedral mechanisms based on polygonal one-degree-of-freedom faces. *Proc IMechE Part C: J Mechanical Engineering Science* 2006; 220: 1011–1018.

[39] Laliberté T and Gosselin CM. Polyhedra with articulated faces. In *Proc. of the 12th IFToMM world congress*.

[40] Kiper G. Fulleroid-like linkages. In *Proceedings of EUCOMES 08*. pp. 423–430.

[41] Röschel O. Overconstrained mechanisms based on trapezohedra. In *Proceedings of the 15th International Conference on Geometry and Graphics (ICGG 2012)*. pp. 629–637.

[42] Kiper G, Söylemez E and Kisisel AUO. Polyhedral linkages synthesized using cardan motion along radial axes. In *Proc. of the 12th IFToMM world congress*. Besancon, France.

[43] Röschel O. Zwangläufig bewegliche polyedermodelle. i. *Mathematica Pannonica* 1995; 6(2): 267–284.

[44] Röschel O. Zwangläufig bewegliche polyedermodelle. ii. *Studia Scientiarum Mathematicarum Hungarica* 1996; 32(3-4): 383–394.

[45] Röschel O. Zwangläufig bewegliche polyedermodelle. iii. *Mathematica Pannonica* 2001; 12(1): 55–68.

[46] Li R, an Yao Y and Kong X. Reconfigurable deployable polyhedral mechanism based on extended parallelogram mechanism. *Mechanism and Machine Theory* 2017; 116: 467–480.

[47] R L, Y Y and X K. *A Method for Constructing Reconfigurable Deployable Polyhedral Mechanism. In: Ding X., Kong X., Dai J. (eds) Advances in Reconfigurable Mechanisms and Robots II. Mechanisms and Machine Science*. Switzerland: Springer, 2016.

[48] Li R, an Yao Y and Kong X. A class of reconfigurable deployable platonic mechanisms. *Mechanism and Machine Theory* 2016; 105: 409 – 427.

[49] Li R, an Yao Y and Ding X. A family of reconfigurable deployable polyhedral mechanisms based on semiregular and johnson polyhedra. *Mechanism and Machine Theory* 2018; 126: 344 – 358.

[50] Wei G and Dai JS. A spatial eight-bar linkage and its association with the deployable platonic mechanisms. *Journal of Mechanisms and Robotics* 2014; 6(2): 021010–021010–9.

[51] Wei G, Ding X and Dai JS. Mobility and geometric analysis of the hoberman switch-pitch ball and its variant. *Transactions of the ASME: Journal of Mechanisms and Robotics* 2010; 2(3): 031010.

[52] Wei G and Dai JS. Synthesis of a family of regular deployable polyhedral mechanisms. In Lenarčič J and Husty M (eds.) *Latest Advances in Robot Kinematics*. Springer, 2012. pp. 123–130.

[53] Wei G and Dai JS. Overconstrained mechanisms with radially reciprocating motion. In Lenarčič J and Stanišić M (eds.) *Advances in Robot Kinematics: Motion in Man and Machine*. Springer, 2010.

[54] Wei G and Dai JS. Synthesis and construction of a family of one-dof highly overconstrained deployable polyhedral mechanisms (dpms). In *2012 Conference proceeding of Design Engineering Technical Conferences & Computers and Information in Engineering Conference*.

[55] Wei G and Dai JS. *Reconfigurable and deployable platonic mechanisms with a variable revolute joint, Advances in Robot Kinematics*. Springer, 2014.

[56] Wohlhart K. Regular polyhedral linkages. In *Proc. 3rd IFToMM International Workshop on Computational Kinematics*. Seoul, South Korea, p. 22. Http://www-sop.inria.fr/coprin/EJCK/Vol1-1/.

[57] Kiper G. Fulleroid-like linkages. In Ceccarelli M (ed.) *Proc. EUCOMES 08*.

[58] Röschel O. A fulleroid-like mechanism based on the cube. *Journal for Geometry and Graphics* 2012; 16(1): 19–27.

[59] Lipkin H. A note on Denavit-Hartenberg notation in robotics. In *ASME 2005 International Design Engineering Technical Conferences & Computers and Information in Engineering Conference*. Long Beach, California USA, p. 85460.

[60] Dai JS, Huang Z and Lipkin H. Mobility of overconstrained parallel mechanisms. *Transactions of the ASME: Journal of Mechanical Design* 2006; 128: 220–229.

[61] Davies T. Kirchhoff's circulation law applied to multi-loop kinematic chains. *Mechanism and Machine Theory* 1981; 16(3): 171–183.

[62] SMintchev LR LDaler and DFloreano. Foldable and self-deployable pocket sized quadcopter. In *IEEE International Conference on Robotics and Automation (ICRA)*. pp. 2190–2195.

[63] Xiu H, Xu T, Wei G et al. Dynamic modelling and simulation of a deployable quadrotor. In *International Conference on Reconfigurable Mechanisms and Robots*. p. 10.1109/REMAR.2018.8449892.

Appendix A

Hereafter, s and c respectively stand for sine and cosine functions.

$$p_{B1} = a_1 \sin\theta_{11} \cos(\varphi/2) \tag{41}$$

$$q_{B1} = a_1 \sin\theta_{11} \sin(\varphi/2) \tag{42}$$

$$r_{B1} = -h - a_1 \cos\theta_{11} \tag{43}$$

$$p_{C1} = a_1 c(\varphi/2) s\theta_{11} + a_2 c(\varphi/2) s(\theta_{11} + \theta_{12}) \tag{44}$$

$$q_{C1} = a_1 s(\varphi/2) s\theta_{11} + a_2 s(\varphi/2) s(\theta_{11} + \theta_{12}) \tag{45}$$

$$r_{C1} = -h - a_1 c\theta_{11} - a_2 c(\theta_{11} + \theta_{12}) \tag{46}$$

$$p_{D1} = a_1 c(\varphi/2) s\theta_{11} + a_2 c(\varphi/2) s(\theta_{11} + \theta_{12}) + a_3 c(\varphi/2) s(\theta_{11} + \theta_{12} + \theta_{13}) \tag{47}$$

$$q_{D1} = a_1 s(\varphi/2) s\theta_{11} + a_2 s(\varphi/2) s(\theta_{11} + \theta_{12}) + a_3 s(\varphi/2) s(\theta_{11} + \theta_{12} + \theta_{13}) \tag{48}$$

$$r_{D1} = -h - a_1 c\theta_{11} - a_2 c(\theta_{11} + \theta_{12}) - a_3 c(\theta_{11} + \theta_{12} + \theta_{13}) \tag{49}$$

$$p_{B2} = a_1 \sin\theta_{21} \cos(\varphi/2) \tag{50}$$

$$q_{B2} = a_1 \sin\theta_{21} \sin(\varphi/2) \tag{51}$$

$$r_{B2} = h + a_1 \cos \theta_{21} \qquad (52)$$

$$p_{C2} = a_1 c\left(\varphi/2\right) s\theta_{21} + a_2 c\left(\varphi/2\right) s\left(\theta_{21} + \theta_{22}\right) \qquad (53)$$

$$q_{C2} = a_1 s\left(\varphi/2\right) s\theta_{21} + a_2 s\left(\varphi/2\right) s\left(\theta_{21} + \theta_{22}\right) \qquad (54)$$

$$r_{C2} = h + a_1 c\theta_{21} + a_2 c\left(\theta_{21} + \theta_{22}\right) \qquad (55)$$

$$p_{D2} = a_1 c\left(\varphi/2\right) s\theta_{21} + a_2 c\left(\varphi/2\right) s\left(\theta_{21} + \theta_{22}\right) + \\ a_3 c\left(\varphi/2\right) s\left(\theta_{21} + \theta_{22} + \theta_{23}\right) \qquad (56)$$

$$q_{D2} = a_1 s\left(\varphi/2\right) s\theta_{21} + a_2 s\left(\varphi/2\right) s\left(\theta_{21} + \theta_{22}\right) + \\ a_3 s\left(\varphi/2\right) s\left(\theta_{21} + \theta_{22} + \theta_{23}\right) \qquad (57)$$

$$r_{D2} = h + a_1 c\theta_{21} + a_2 c\left(\theta_{21} + \theta_{22}\right) + \\ a_3 c\left(\theta_{21} + \theta_{22} + \theta_{23}\right) \qquad (58)$$

Appendix B

$$\mathbf{R}_1 = \begin{bmatrix} -\frac{\sqrt{2}}{2}c\theta - \frac{\sqrt{6}}{6}s\theta & \frac{\sqrt{2}}{2}s\theta - \frac{\sqrt{6}}{6}c\theta & -\frac{\sqrt{3}}{3} \\ -\frac{\sqrt{6}}{3}s\theta & -\frac{\sqrt{6}}{3}c\theta & \frac{\sqrt{3}}{3} \\ \frac{\sqrt{6}}{6}s\theta - \frac{\sqrt{2}}{2}c\theta & \frac{\sqrt{6}}{6}c\theta + \frac{\sqrt{2}}{2}s\theta & \frac{\sqrt{3}}{3} \end{bmatrix} \qquad (59)$$

$$\mathbf{R}_2 = \begin{bmatrix} \frac{\sqrt{2}}{2}c\theta - \frac{\sqrt{6}}{6}s\theta & -\frac{\sqrt{2}}{2}s\theta - \frac{\sqrt{6}}{6}c\theta & -\frac{\sqrt{3}}{3} \\ -\frac{\sqrt{6}}{6}s\theta - \frac{\sqrt{2}}{2}c\theta & -\frac{\sqrt{6}}{6}c\theta + \frac{\sqrt{2}}{2}s\theta & -\frac{\sqrt{3}}{3} \\ \frac{\sqrt{6}}{3}s\theta & \frac{\sqrt{6}}{3}c\theta & -\frac{\sqrt{3}}{3} \end{bmatrix} \qquad (60)$$

$$\mathbf{R}_3 = \begin{bmatrix} -\frac{\sqrt{6}}{3}s\theta & -\frac{\sqrt{6}}{3}c\theta & \frac{\sqrt{3}}{3} \\ \frac{\sqrt{2}}{2}c\theta - \frac{\sqrt{6}}{6}s\theta & -\frac{\sqrt{2}}{2}s\theta - \frac{\sqrt{6}}{6}c\theta & -\frac{\sqrt{3}}{3} \\ \frac{\sqrt{6}}{6}s\theta + \frac{\sqrt{2}}{2}c\theta & \frac{\sqrt{6}}{6}c\theta - \frac{\sqrt{2}}{2}s\theta & \frac{\sqrt{3}}{3} \end{bmatrix} \qquad (61)$$

$$\mathbf{R}_4 = \begin{bmatrix} \frac{\sqrt{2}}{2}c\theta + \frac{\sqrt{6}}{6}s\theta & -\frac{\sqrt{2}}{2}s\theta + \frac{\sqrt{6}}{6}c\theta & \frac{\sqrt{3}}{3} \\ -\frac{\sqrt{6}}{3}s\theta & -\frac{\sqrt{6}}{3}c\theta & \frac{\sqrt{3}}{3} \\ -\frac{\sqrt{6}}{6}s\theta + \frac{\sqrt{2}}{2}c\theta & -\frac{\sqrt{6}}{6}c\theta - \frac{\sqrt{2}}{2}s\theta & -\frac{\sqrt{3}}{3} \end{bmatrix} \qquad (62)$$

$$\boldsymbol{p}_1 = d\begin{bmatrix} -\sqrt{3}/3 & \sqrt{3}/3 & \sqrt{3}/3 \end{bmatrix}^{\mathrm{T}} \qquad (63)$$

$$\boldsymbol{p}_2 = d\begin{bmatrix} -\sqrt{3}/3 & -\sqrt{3}/3 & -\sqrt{3}/3 \end{bmatrix}^{\mathrm{T}} \qquad (64)$$

$$\boldsymbol{p}_3 = d\begin{bmatrix} \sqrt{3}/3 & -\sqrt{3}/3 & \sqrt{3}/3 \end{bmatrix}^{\mathrm{T}} \qquad (65)$$

$$\boldsymbol{p}_4 = d\begin{bmatrix} \sqrt{3}/3 & \sqrt{3}/3 & -\sqrt{3}/3 \end{bmatrix}^{\mathrm{T}} \qquad (66)$$

Appendix C

$$\mathbf{M}_{11} = \begin{bmatrix} S_{11} & S'_{11} & 0 & 0 & S_{13} & S'_{13} \\ 0 & 0 & 0 & 0 & 0 & 0 \\ -S_{11} & -S'_{11} & S_{12} & S'_{12} & 0 & 0 \end{bmatrix} \qquad (67)$$

$$\mathbf{M}_{12} = \begin{bmatrix} S_{21} & S'_{21} & S_{22} & S'_{22} & 0 & 0 \\ -S_{21} & -S'_{21} & 0 & 0 & S_{23} & S'_{23} \\ 0 & 0 & 0 & 0 & 0 & 0 \end{bmatrix} \qquad (68)$$

$$\mathbf{M}_{13} = \begin{bmatrix} 0 & 0 & 0 & 0 & 0 & 0 \\ S_{31} & S'_{31} & S_{32} & S'_{32} & 0 & 0 \\ -S_{31} & -S'_{31} & 0 & 0 & S_{33} & S'_{33} \end{bmatrix} \qquad (69)$$

$$\mathbf{M}_{21} = \begin{bmatrix} 0 & 0 & -S_{12} & -S'_{12} & -S_{13} & -S'_{13} \\ 0 & 0 & 0 & 0 & 0 & 0 \end{bmatrix} \qquad (70)$$

$$\mathbf{M}_{22} = \begin{bmatrix} 0 & 0 & 0 & 0 & 0 & 0 \\ 0 & 0 & -S_{22} & -S'_{22} & -S_{23} & -S'_{23} \end{bmatrix} \qquad (71)$$

$$\mathbf{M}_{24} = \begin{bmatrix} 0 & 0 & S_{42} & -S'_{42} & S_{43} & S'_{43} \\ S_{41} & S'_{41} & -S_{42} & -S'_{42} & 0 & 0 \end{bmatrix} \qquad (72)$$